Proc. NIPR Symp. Antarct. Meteorites, 4, 187–225, 1991

PETROLOGY AND MINERALOGY OF THE YAMATO-82162 CHONDRITE (CI)

Yukio IKEDA

Department of Earth Sciences, Faculty of Science, Ibaraki University, 1–1, Bunkyo 2-chome, Mito 310

Abstract: Yamato-82162 (Y-82162) is a regolith breccia including many kinds of clasts. The clasts are classified into 6 clast-types on the basis of the predominant phase and the textures. They are phyllosilicate, carbonate, unusual, magnetite, composite, and matrix-like clast-types. The phyllosilicate clasts are subdivided into two subtypes, sodian talc-rich and chlorite-rich. The sodian talc-rich clasts consist mainly of sodian talc and minor chlorite (or serpentine), and they are coarse-grained and homogeneous in chemical composition. They seem to have formed in hot and deep interior of the parent body. Chlorite-rich clasts, magnetite clasts, and matrix-like clasts consist mainly of chlorite and minor sodian talc, and they show unique microtextures; amygdule, network-like, and microspherulitic. The three clast-types seem to have formed near the surface of the parent body. Matrix-like and composite clasts are sometimes cut across by phyllosilicate veins, which may have been formed by a fluid coming from the interior of the parent body where sodian talc-rich clasts were produced. The unusual clasts include FeO-bearing periclase which sometimes overgrows on magnetite grains and is rimmed by an unknown Fe-Ca-S-O phase, suggesting that the unusual clasts were produced from carbonate-rich precursors by heating events. In addition to these clasts, Y-82162 includes anhydrous chondritic fragments, which were projectiles collided on the parent body to have produced the regolith breccia of Y-82162.

1. Introduction

The Yamato-82162 (Y-82162) chondrite is one of the three carbonaceous chondrites which have been studied by the consortium of the Antarctic carbonaceous chondrites with CI affinities, Yamato-82162, Yamato-86720, and Belgica-7904. The Y-82162 chondrite has already been studied by many consortium members. Mineralogy and petrology: KOJIMA and YANAI (1987), TOMEOKA *et al.* (1988, 1990), WATANABE *et al.* (1988), AKAI (1989, 1990), BISCHOFF and METZLER (1990), and IKEDA (1990), chemistry; KALLEMEYN (1988), YAMAMOTO and NAKAMURA (1989), PAUL and LIPSCHUTZ (1989, 1990), and EBIHARA and SHINONAGA (1989), reflectance spectral analyses; MIYAMOTO (1990), and oxygen isotopic composition; MAYEDA and CLAYTON (1987, 1990) and CLAYTON and MAYEDA (1989).

Y-82162 is considered to be a CI chondrite from petrological, chemical and oxygen isotopic points of view. However, this chondrite shows several characteristics different from those of non-Antarctic CI chondrites. They are as follows: (1) The water content of Y-82162 (11.95 wt% including carbon content) is lower than those of non-Antarctic CI chondrites (about 20 wt%) (KOJIMA and YANAI, 1987;

TOMEOKA *et al.*, 1989; TOMEOKA, 1990). (2) Some phyllosilicates in Y-82162 include tiny olivine grains which seem to have been produced from the host phyllosilicates by a heating event (AKAI, 1989; TOMEOKA *et al.*, 1989). (3) Although non-Antarctic CI chondrites include many veins consisting mainly of carbonates and/or sulfates, such veins are not found in Y-82162. Instead of carbonate and sulfate veins, phyllosilicate veins are found in Y-82162 (TOMEOKA, 1990). (4) Ubiquitous occurrence of sulfides such as pyrrhotite and less pentlandite is characteristic of Y-82162 (KOJIMA and YANAI, 1987; TOMEOKA *et al.*, 1988; WATANABE *et al.*, 1988). (5) Although the oxygen isotopic composition of Y-82162 is roughly similar to those of non-Antarctic CI chondrites, the former is slightly enriched in heavier oxygen isotopes in comparison to those of non-Antarctic CI chondrites (MAYEDA and CLAYTON, 1987, 1990). (6) The comparison of labile trace element contents of Y-82162 with those of Murchison samples artificially heated suggests that Y-82162 was thermally metamorphosed over the 600–700°C range (PAUL and LIPSCHUTZ, 1989). The above-stated differences between Y-82162 and non-Antarctic CI chondrites indicate that the former has formed in a different way from the latter or has experienced a different thermal history. Detailed studies on Y-82162 may give an important key to the origin of CI chondrites.

Y-82162 is a regolith breccia, including many kinds of clasts set in the matrix (IKEDA, 1990). The purposes of this study are (1) classification of clasts by a dominant phase, mineral assemblages and textures, (2) detailed petrography of all constituents of Y-82162, and (3) to explain the genesis of clasts and genetical relationships among the clasts in Y-82162.

2. Analytical Methods

The chemical compositions of minerals are obtained using an electron-probe micro-analyzer (EPMA). The correction was carried out with the Bence-Albee methods for silicates, oxides, carbonates, and phosphates, and with standard ZAF methods for sulfides and metals. Some kinds of oxides, carbonates and hydroxides were corrected by the standard ZAF methods to give the cation and oxygen contents independently, where synthetic MgO was used as standard for oxygen.

The constituent minerals in the matrix of Y-82162 and fine-grained portions of clasts are too small to obtain the chemical composition of a single grain by an EPMA. Instead of a single grain, average compositions of fine-grained aggregates were obtained by a focussed beam of an EPMA.

3. Sample and Overall Description

Two thin sections of Y-82162 (Y-82162,4–2 and ,4–3) which were borrowed from National Institute of Polar Research were available for the consortium and have been already studied by several consortium members prior to my study. Y-82162 is a regolith breccia, showing a breccia-in-breccia structure. It consists of four distinct units; (1) clasts, (2) isolated minerals, (3) matrix, and (4) anhydrous chondritic fragments. They are summarized in Table 1.

Clasts are millimeters or submillimeters in size, showing irregular or subrounded

Table 1. The constituents of Y-82162.

- Clasts
  - Phyllosilicate clasts ····· Sodian talc-rich clasts / Chlorite-rich clasts
  - Matrix-like clasts
  - Carbonate clasts
  - Unusual clasts ····· CaO-rich unusual clasts / CaO-poor unusual clasts (MnO-rich / MnO-poor)
  - Magnetite clasts
  - Composite clasts
- Isolated minerals ····· Sulfide minerals / Oxide minerals / Phosphate minerals / Others
- Matrix
- Anhydrous chondritic fragments

outlines. They show various kinds of mineral assemblages, textures, and grain sizes. Matrix is defined here to be fine-grained aggergates which fulfill the interstitial spaces among clasts or other constituents. The matrix consists mainly of fine-grained materials smaller than a few microns across, which are not identified under the microscope. Isolated minerals are euhedral or angular grains set in the matrix, which are larger than a few microns across. Anhydrous chondritic fragments are free from hydrous minerals and consist mainly of olivine and pyroxene.

4. Classification and Description of Clasts

Clasts in Y-82162 are classified into six types on the basis of the predominant mineral and/or textures (Table 1). Two types are further divided into two subtypes on the basis of the predominant phase, mineral assemblages, chemistry, and/or textures. The mineral assemblages of each clast-type are summarized in Table 2.

4.1. Phyllosilicate clasts

Phyllosilicates are predominant in this clast-type with subordinate amounts of carbonate, magnetite, apatite and/or pyrrhotite. This clast-type can be divided into two subtypes, sodian talc-rich clasts and chlorite-rich clasts, in which the predominant phases are sodian talc component-rich and chlorite component-rich phyllosilicates, respectively.

Phyllosilicates in sodian talc-rich clasts are coarse-grained, about a few microns wide and a few tens of microns long (Photos 1 and 2). Sodian talc-rich clasts often include euhedral pyrrhotite grains and carbonate nodules (Photo 1). This type is free from magnetite, but apatite, rarely up to about 30 modal %, is found.

Chlorite-rich clasts are coarse- to fine-grained (Photos 3 and 4), and the grain size of the coarse-grained clasts is similar to that of the sodian talc-rich clasts. Sometimes they show a remarkable amygdule texture (Photo 4). Some chlorite-rich clasts include large amounts of apatite and/or magnetite in addition to pyrrhotite.

4.2. Matrix-like clasts

Matrix-like clasts (Photos 5, 6, 7, and 8) are similar in texture and mineral as-

Table 2. Mineral assemblages of clasts, isolated minerals, matrix, and anhydrous chondritic fragments in the Y-82162 carbonaceous chondrite.

	Sodian talc clasts	Chlorite clasts	Carbonate clasts	Ca-rich unusual clasts	Mn-rich unusual clasts	Magnetite clasts	Sulfide minerals	Oxide minerals	Matrix	Anhydrous chondritic fragments
Sodian talc	+++	+								
Chlorite (or serpentine)	+	+++				+			+++	
MnO-rich chlorite				+						
Ankerite	+	+	+++	+						
Dolomite			+	+		+				
Rhodochrosite					+					
Mn-rich magnetite			+	+	+			+		
Mn-poor magnetite		+				+++		+		
Ilmenite								+		
Periclase				+						
Alpha phase				+						
PCA aggregate			+	+++						
PER aggregate				+	+++					
PMN aggregate					+++					
Apatite	+	+	+	+		+				
Pyrrhotite	+	+	+	+	+		+			
Pentlandite							+			
Chalcopyrite							+			
Awaruite							+			
Ferrihydrite							+			
Olivine										+
Low-Ca pyroxene										+
Augite										+
Fassaite										+
Sodic plagioclase										+
Chromite										+
Whitlockite										+
Troilite										+

Alpha phase has a chemical composition similar to 15FeS·16 (Ca, Fe) O with a small amount of P_2O_5. PCA, PER, and PMN are fine-grained aggregates of (Mg-Fe mono-oxides and Ca-rich carbonates), (FeO-poor periclase, FeS, and probably magnetite), and (FeO-poor periclase, FeS, rhodochrosite, and probably magnetite), respectively.
Abundant (+++) and common (+).

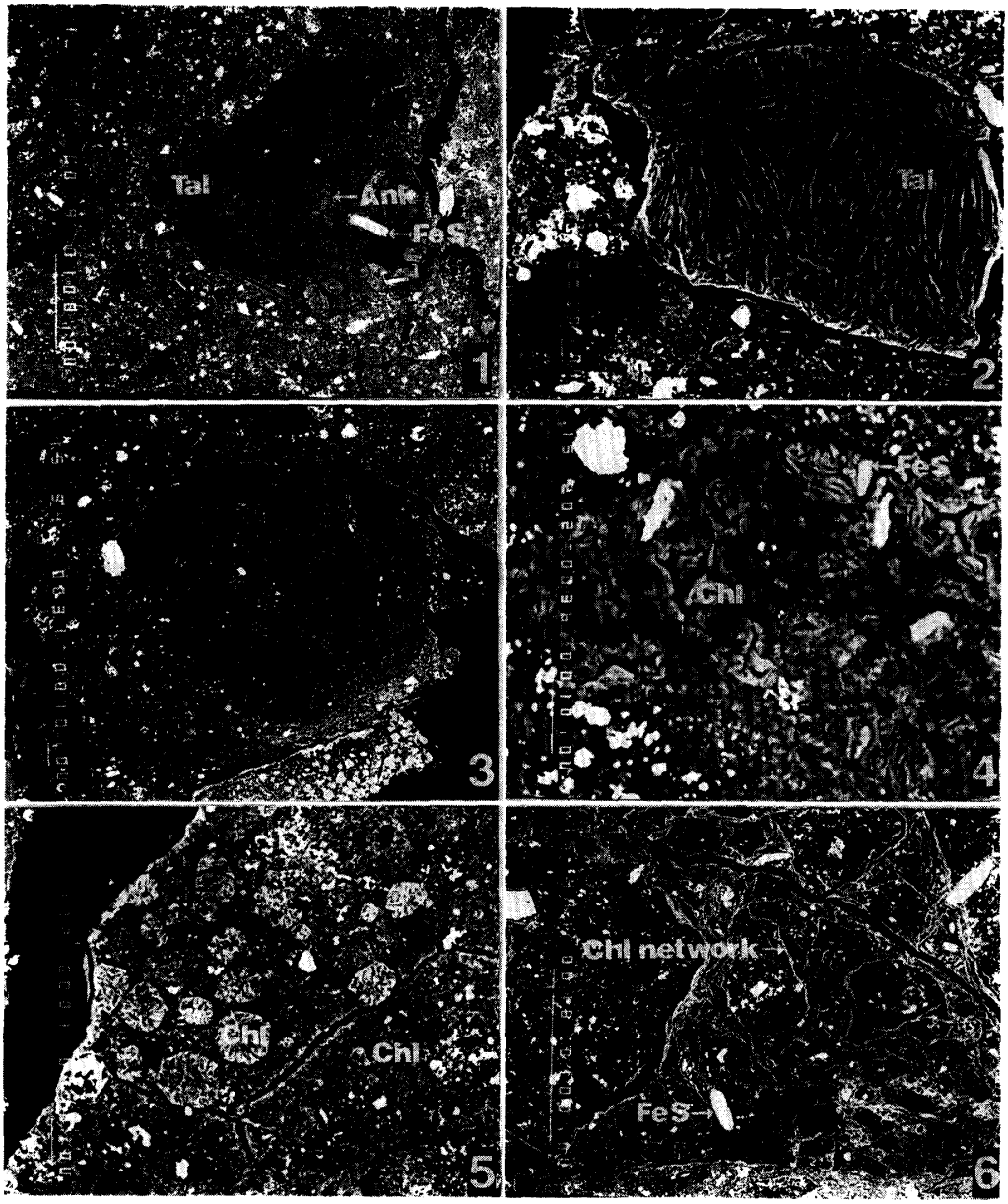

Microphotographs of all clast-types, isolated mineral fragments, matrix, and anhydrous chondritic fragments in Y-82162. All photographs are back-scattered electron (BSE) images.

Photo 1. A sodian talc-rich phyllosilicate clast. Note that it consists of coarse-grained sodian talc-rich phyllosilicates (Tal), including ankerite nodules (Ank) and euhedral pyrrhotite grains (FeS). White bar at the left is 100 microns.

Photo 2. A sodian talc-rich phyllosilicate clast. Note the coarse-grained phyllosilicates (Tal). White bar at the left is 10 microns.

Photo 3. A chlorite-rich phyllosilicate clast. White bar at the left is 10 microns.

Photo 4. A portion of a chlorite-rich phyllosilicate clast. Note amygdule texture of chlorite (Chl) and euhedral pyrrhotite grains (FeS). White bar at the left is 10 microns.

Photo 5. A portion of a matrix-like clast. Note chlorite spherules (Chl at the center) occurring in fine-grained massive chlorite (or serpentine) aggregates (Chl at the right). White bar at the left is 10 microns.

Photo 6. A portion of a matrix-like clast. Note the chlorite networks (Chl network) and euhedral pyrrhotite grains (FeS). White bar at the left is 100 microns.

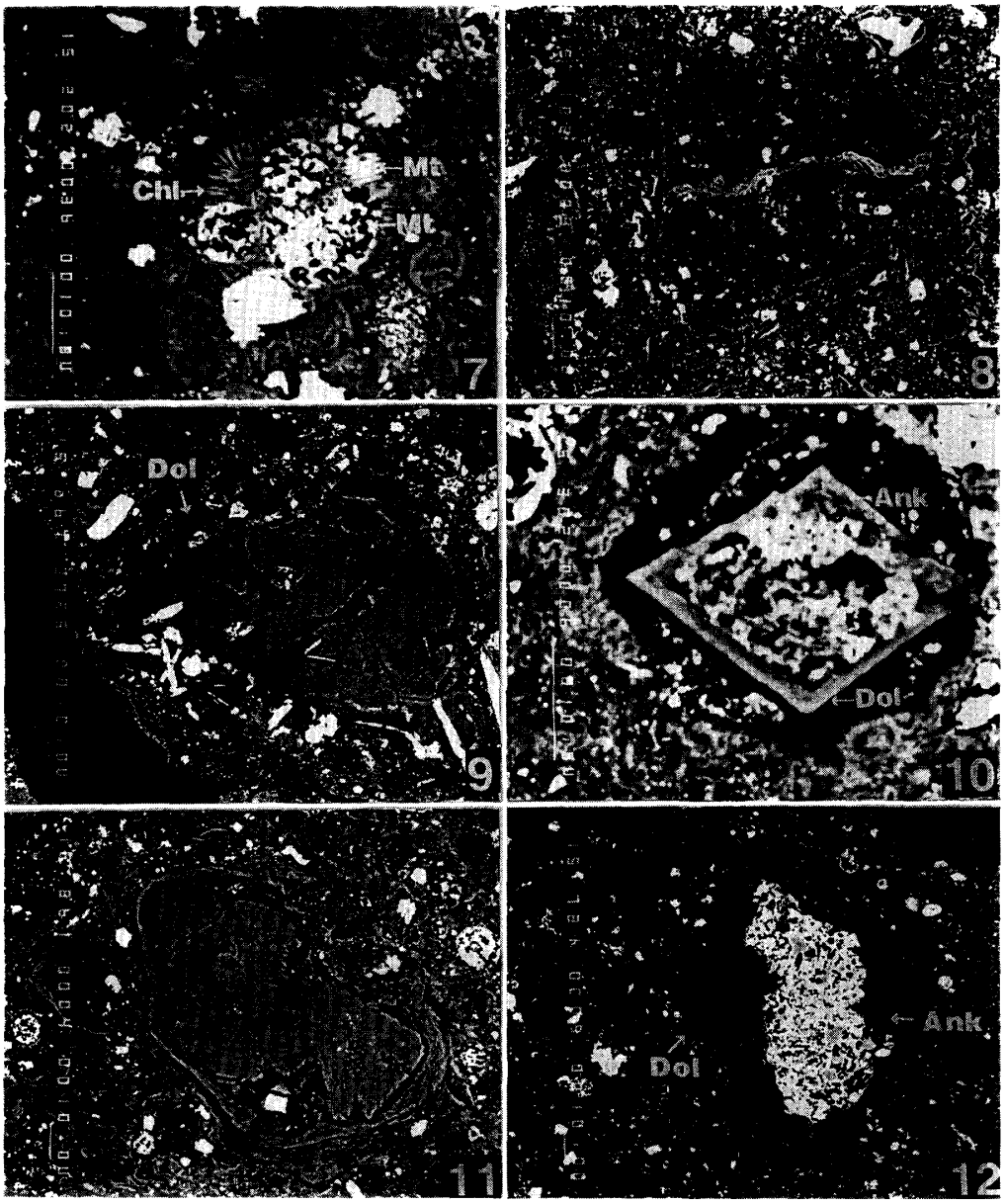

Photo 7. A portion of a matrix-like clast. Note the chlorite spherule (Chl) including magnetite framboids (Mt, lower) and plaquettes (Mt, upper). White bar at the left is 10 microns.

Photo 8. A matrix-like clast. Note that a phyllosilicate vein cut across the matrix-like clast. White bar at the left is 10 microns.

Photo 9. A carbonate clast. Small magnetite grains and pyrrhotite laths are included in the core and peripheral portions, respectively. Note that a thin dolomite rim (Dol) completely surrounds the clast. White bar at the left is 10 microns.

Photo 10. A carbonate clast. Note the euhedral outline of the clast and a thin dolomite rim (Dol) surrounding the ankeritic carbonates (Ank). White bar at the left is 10 microns.

Photo 11. A carbonate clast. Ankerite (Ank) includes an rectangular MnO-rich magnetite (Mt) at the lower portion. Note the phyllosilicate rim (Tal) completely surrounding the clast. White bar at the left is 10 microns.

Photo 12. A CaO-rich unusual clast. The oxide core is completely surrounded by an ankerite mantle (Ank), which is in turn surrounded by a thin dolomite rim (Dol). White bar at the left is 10 microns.

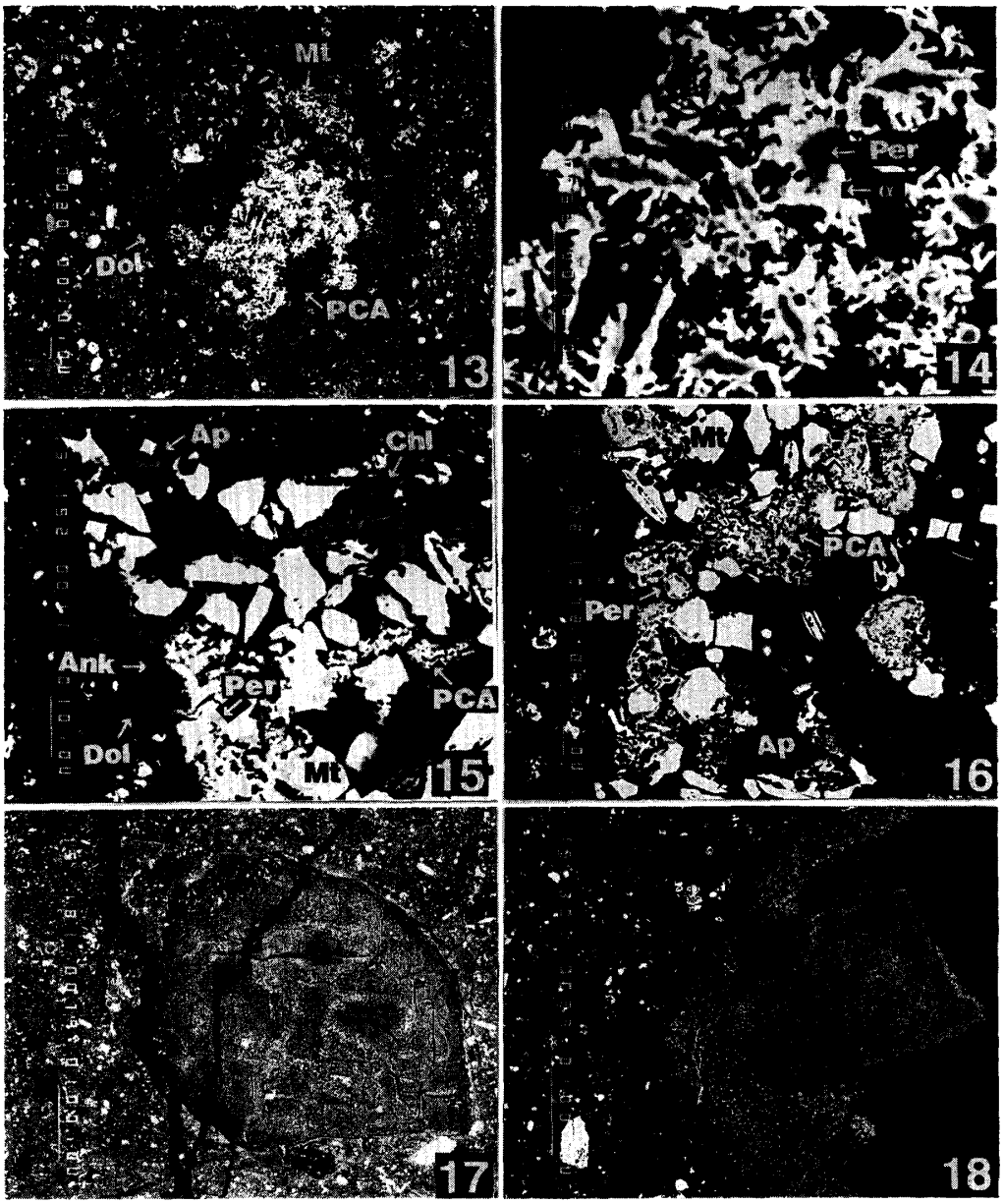

Photo 13. A CaO-rich unusual clast consisting mainly of periclase, alpha phase and PCA aggregate. Note that framboidal magnetites (Mt) occur in the upper portion. White bar at the left is 10 microns.

Photo 14. Enlarged image of Photo 13. Dark periclase grains (Per) are completely surrounded by alpha phase. White bar at the left is 10 microns.

Photo 15. A portion of a unique clast (No. 41) of CaO-rich unusual clast-type. MnO-rich chlorites (Chl) occur in association with irregular magnetite grains (Mt). An apatite grain (Ap) includes a rectangular magnetite in the upper portion. Note that periclase (Per) and PCA aggregate (PCA) never occur in the chlorites. Ankerite mantle (Ank) and dolomite rim (Dol) are observed at the left portion. White bar at the left is 10 microns.

Photo 16. The same clast as that of Photo 15. Note that periclase (Per) overgrows on magnetite grains (Mt) which are not surrounded by apatites (Ap), and that alpha phase rims the periclase. White bar at the left is 10 microns.

Photo 17. MnO-rich subtype of CaO-poor clasts. Dark groundmass and bright mottles are fine-grained PER and PMN aggregates, respectively. White bar at the left is 10 microns.

Photo 18. MnO-rich subtype of CaO-poor unusual clasts. White bar at the left is 100 microns.

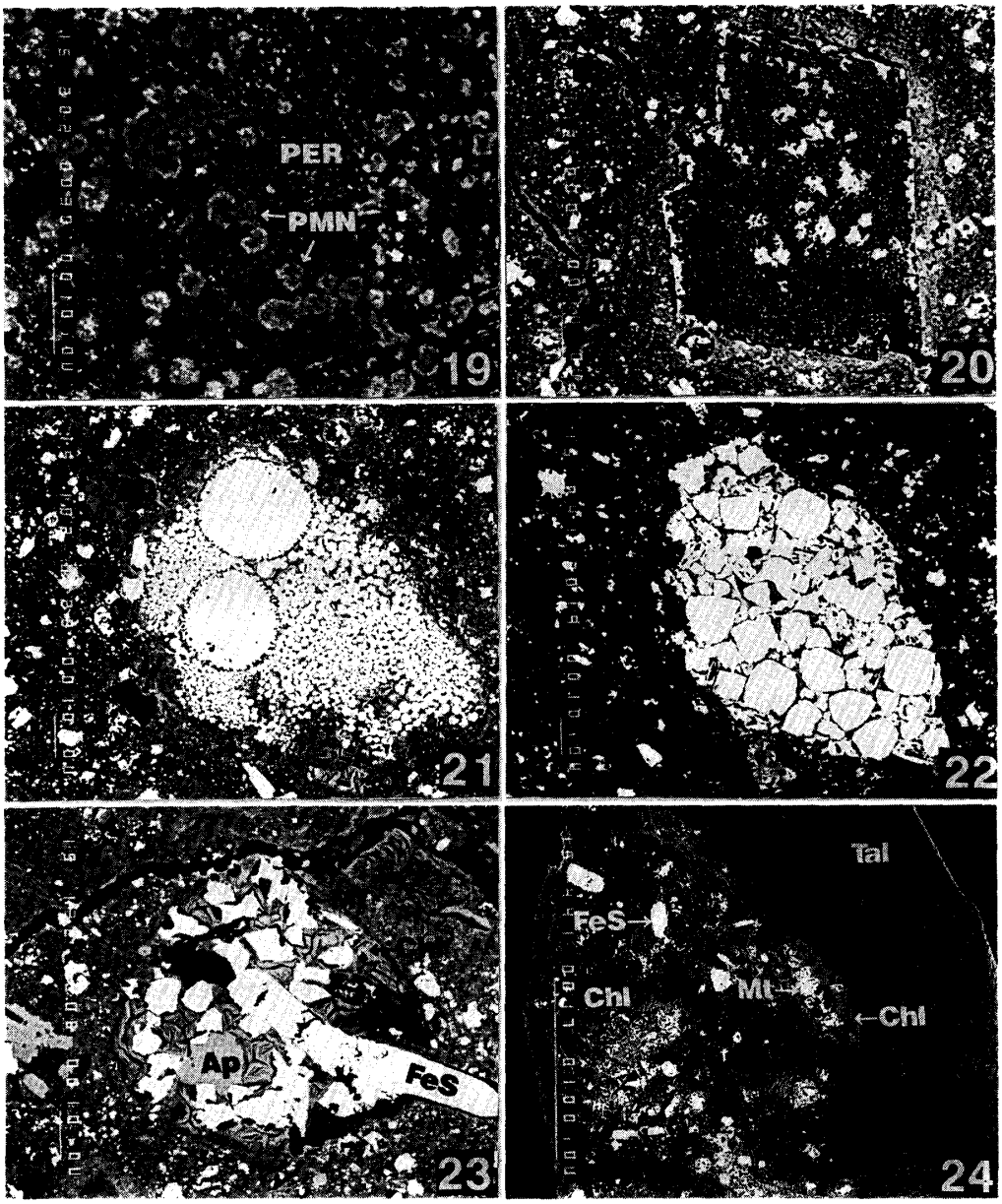

Photo 19. Enlarged image of Photo 18. Bright mottles of PMN aggregate occur in fine-grained massive PER aggregates. White bar at the left is 10 microns.

Photo 20. MnO-poor subtype of CaO-poor unusual clasts. Pyrrhotite grains (bright phase) occur in fine-grained PER aggregate and at the rim of the clast. White bar at the left is 10 microns.

Photo 21. A magnetite clast. Two large magnetite spherules occur in magnetite framboids. In the interstitial spaces among the magnetite framboids, chlorite-rich phyllosilicates show amygdule textures. White bar at the left is 10 microns.

Photo 22. A magnetite clast. Subrounded grains and plaquettes of magnetites are observed. White bar at the left is 10 microns.

Photo 23. Intermediate type between magnetite and chlorite-rich clast-types. Note subrounded magnetite grains (Mt) and interstitial chlorite-rich phyllosilicates (Chl) showing amygdule textures. Apatite (Ap) and pyrrhotite (FeS) are included. White bar at the left is 10 microns.

Photo 24. A portion of a composite clast. The right portion is a sodian talc-rich phyllosilicates, and the left portion is a matrix-like clast. Note that sodian talc-rich phyllosilicates (Tal) which are directly in contact with magnetite grains (Mt) become FeO-rich chlorites (Chl with an arrow). White bar at the left is 100 microns.

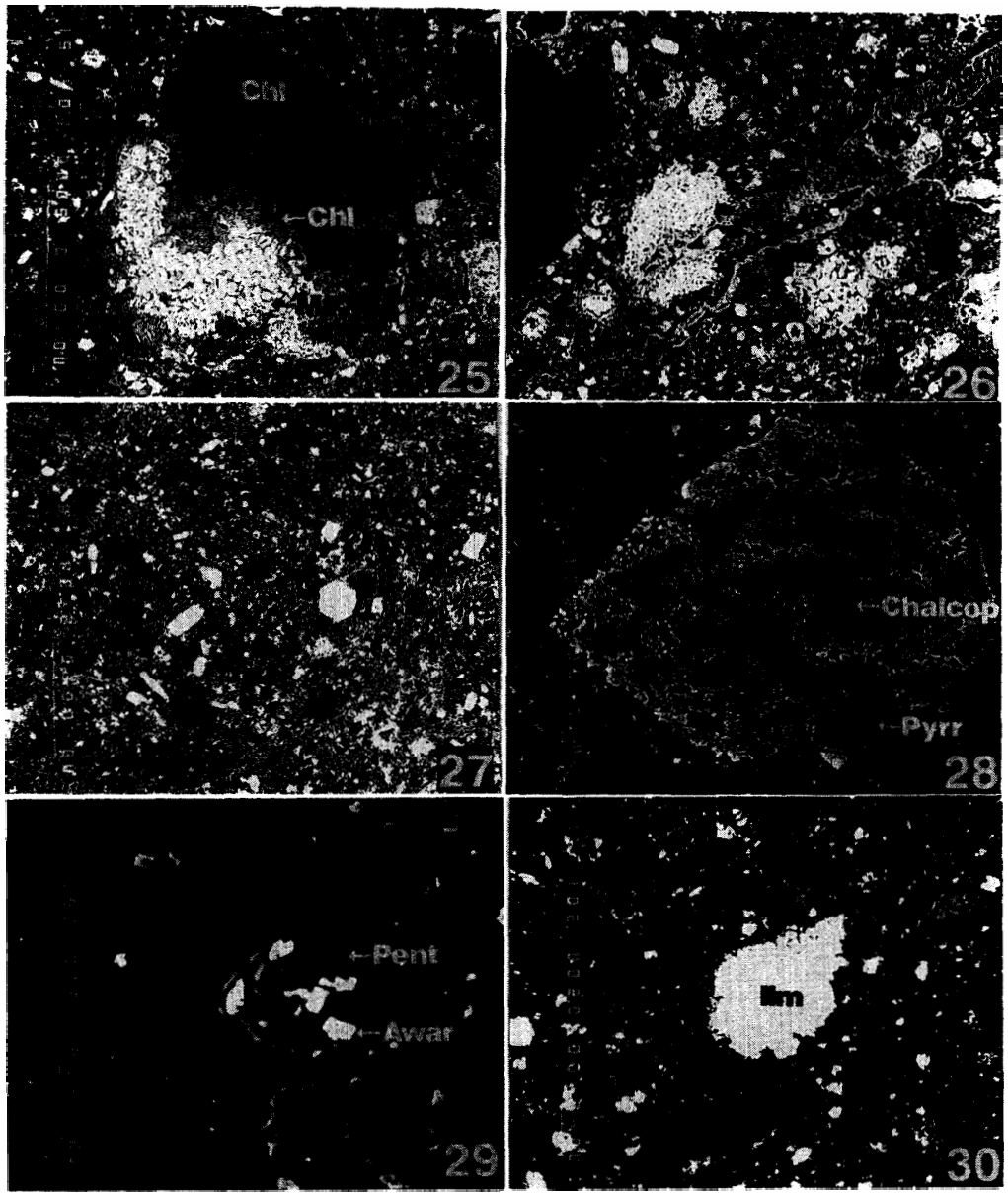

Photo 25. A composite clast. This consists of a coarse-grained chlorite-rich clast and a magnetite clast. Note that chlorite-rich phyllosilicates which are directly in contact with the magnetite clast become FeO-rich chlorites (Chl with an arrow). White bar at the left is 100 microns.

Photo 26. A portion of a composite clast. This clast is cut across by a phyllosilicate vein which sometimes branches out. The vein phyllosilicates which are directly in contact with magnetite framboids (central left) become FeO-rich chlorites. White bar at the left is 10 microns.

Photo 27. Isolated pyrrhotite grains setting in the matrix. Note the euhedral laths and hexagonal outlines of pyrrhotite showing that they have originally crystallized as hexagonal pyrrhotites. White bar at the left is 10 microns.

Photo 28. Isolated sulfide minerals. This consists of an intergrowth of chalcopyrite (Chalcop) and pyrrhotite (Pyrr) in nearly equal amounts. White bar at the left is 10 microns.

Photo 29. Isolated minerals of pentlandite (Pent) including small awaruite grains (Awar). White bar at the left is 10 microns.

Photo 30. An isolated ilmenite grain (Ilm) with ragged rim. White bar at the left is 10 microns.

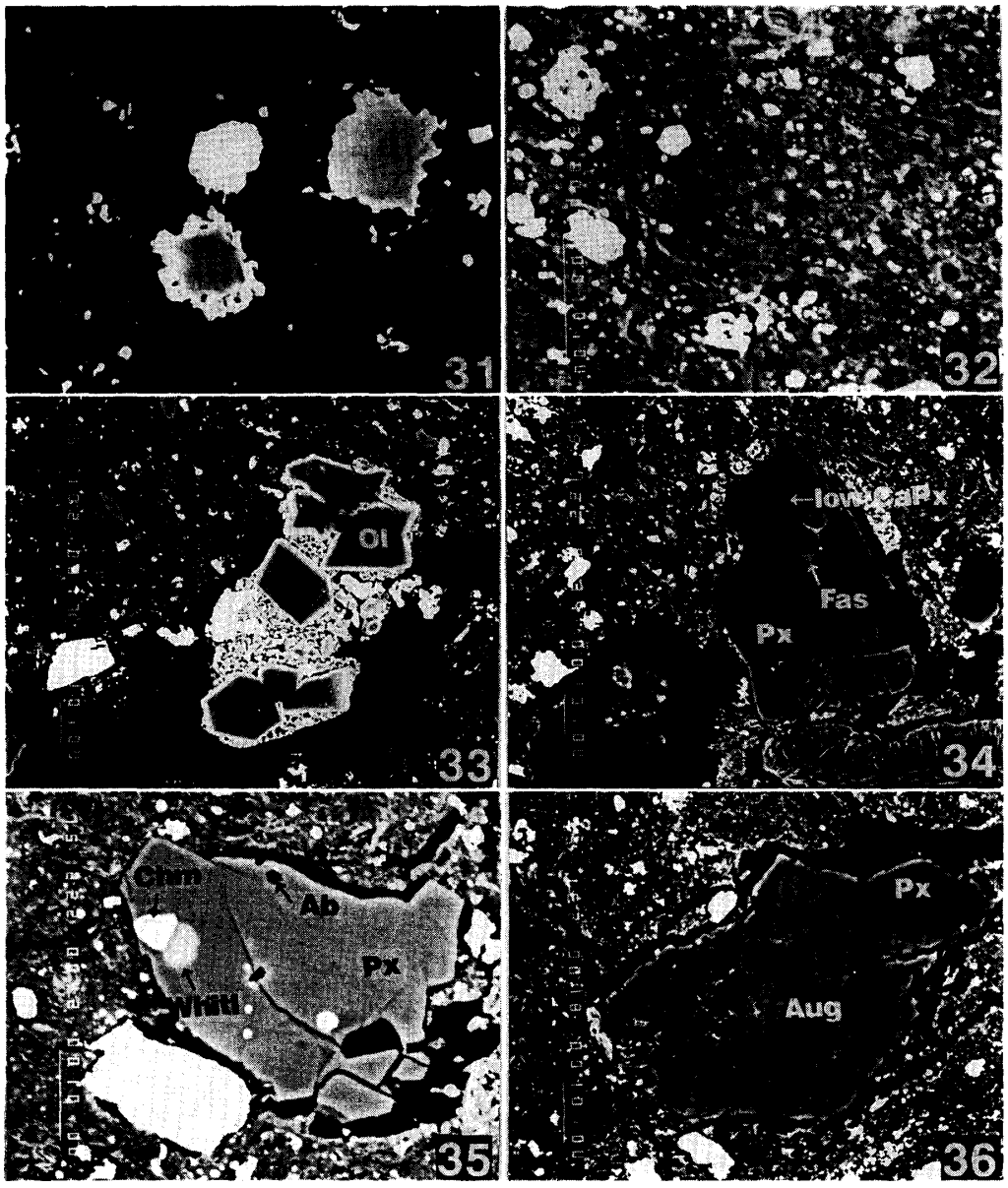

Photo 31. Isolated magnetite grains in the matrix. Note that the magnetite (darker phase) is surrounded by pyrrhotite (brighter rim). White bar at the left is 10 microns.

Photo 32. The matrix showing the fine-grained massive aggregates of phyllosilicates with pyrrhotite and magnetite grains. White bar at the left is 10 microns.

Photo 33. An anhydrous chondritic fragment. Olivine (Ol) shows a chemical zoning from magnesian cores to ferroan rims. White bar at the left is 10 microns.

Photo 34. An anhydrous chondritic fragment. Low-Ca pyroxene (Px) includes very-low-Ca pyroxene (lowCaPx, this was originally protoenstatite), and fassaite (Fas) occurs in the interstitial space. White bar at the left is 10 microns.

Photo 35. An anhydrous chondritic fragment. Orthopyroxene (Px) includes small grains of chromite (Chm), whitlockite (Whitl), and albitic plagioclase (Ab). White bar at the left is 10 microns.

Photo 36. An anhydrous chondritic fragment. This consists of low-Ca pyroxene (Px) and augite (Aug). White bar at the left is 10 microns.

semblage to the matrix of Y-82162. However, careful observation of these clasts under the microscope reveals that they are sometimes different in microtextures from the matrix. Four types of microtextures are observed in matrix-like clasts. They are network-like, microspherulitic, vein-like and fine-grained massive aggregates, and most matrix-like clasts show two or three types of the four microtextures in one clast. A matrix-like clast (Photo 6) consists of massive matrix-like materials and chlorite-networks. Another clast (Photo 5) shows a microspherulitic texture, in which chlorite spherules, several up to a few tens of microns across, show radial sheef-like aggregate of chlorite with thin chorite rims. Sometimes large chlorite spherules include a magnetite aggregate and/or magnetite plaquette (Photo 7). A massive chlorite-rich clast is shown in Photo 8, where the clast is cross-cut by a phyllosilicate vein.

4.3. Carbonate clasts

Carbonate clasts consist mainly of carbonates with subordinate and various amounts of magnetite, pyrrhotite, and so on. There are dolomite-rimmed and dolomite-rim-free clasts. Dolomite-rimmed clasts are partially or wholly surrounded by a thin rim of dolomite, a few microns in width (Photo 9). Rarely dolomite-rimmed clasts show a rhombic outline (Photo 10). Dolomite-rim-free clasts are sometimes surrounded by a thin rim of sodian talc-rich phyllosilicates (Photo 11).

4.4. Unusual clasts

Unusual clasts in Y-82162 have a unique core-mantle structure which is not observed in the other clast-types, or have unusual textures consisting of heterogeneous fine-grained aggergates. This type is divided into two types; CaO-rich and CaO-poor (Table 1). The CaO-rich unusual clasts consist mainly of MgO-FeO oxides such as periclase and Ca-rich carbonates such as ankerite and dolomite. They often show a core-mantle structure (Photo 12); the core consists mainly of FeO-bearing periclase, an unknown Fe-Ca-S-O phase (hereafter, alpha phase), and very fine-grained aggregates consisting mainly of periclase and Ca-rich carbonate (hereafter, PCA aggregate) with variable amounts of sulfide and magnetite (Photo 13). The FeO-bearing periclase grains are a few to several microns across, and always surrounded by a rim of the alpha phase, from a few to several microns in width (Photo 14). The mantle consists mainly of Ca-rich carbonates, and the outermost thin rim of dolomite partially or wholly surrounds the mantle carbonates.

One clast is a unique type of CaO-rich unusual clast, which includes large amounts of magnetite, apatite, and minor chlorite-rich phyllosilicates (Photos 15 and 16).

CaO-poor unusual clasts are fine-grained aggregates of MgO-FeO oxides with variable amounts of Ca-poor carbonates. They have no core-mantle structure. The CaO-poor unusual clasts are further divided into two subtypes, MnO-rich and MnO-poor (Table 1). The former subtype includes two kinds of very fine-grained aggregates, MgO-FeO aggregates consisting mainly of periclase (hereafter, PER aggregate) and Mn-rich aggregates consisting mainly of periclase and Mn-rich carbonate (hereafter, PMN aggregate) (Photos 17, 18, and 19), and the latter subtype consists mainly of MgO-FeO aggregates (PER aggregate) with FeS grains (Photo 20).

4.5. Magnetite clasts

Magnetite clasts consist mainly of magnetites with variable amounts of chlorite-rich phyllosilicates, apatite, and pyrrhotite. Magnetites show various textures; framboidal, spherulitic, plaquette, and irregular. Photo 21 is a clast consisting of framboidal magnetite and interstitial chlorite-rich phyllosilicates, and the phyllosilicates show an amygdule texture. Photo 22 is a magnetite clast consisting of irregular and plaquette magnetites and interstitial chlorite-rich phyllosilicates with a small amount of apatite. One clast (Photo 23) consists of chlorite-rich phyllosilicates and irregular magnetite with minor amounts of pyrrhotite and apatite, and is an intermediate type between chlorite-rich clasts and magnetite clasts.

4.6. Composite clasts

Composite clasts include two or more clast-types. Photo 24 is a composite clast consisting of a sodian talc-rich clast and a matrix-like clast. One composite clast (Photo 25) consists of a chlorite-rich clast and a magnetite clast. Some composite clasts are cut through by phyllosilicate veins, the width being a few to a few tens of microns (Photo 26). Sometimes they have branches which turn off.

5. Isolated Minerals, Matrix, and Anhydrous Chondritic Fragments

5.1. Isolated minerals

Isolated minerals occur directly in the matrix of Y-82162 and in matrix-like clasts. The most common is pyrrhotite (or troilite), which often shows a euhedral hexagonal outline (Photo 27). Rarely pyrrhotite occurs as intergrown with chalcopyrite (Photo 28). Pentlandite as an isolate mineral sometimes includes small grains of awaruite (Photo 29). Ilmenite grains are large, up to several tens of microns across, show an irregular outline (Photo 30). Phyllosilicates, carbonates, magnetite, apatite and so on occur as isolated minerals and may have been derived from broken clasts. Small magnetite grains in the matrix are sometimes surrounded by pyrrhotite rims (Photo 31).

5.2. Matrix

The matrix of Y-82162 is very fine-grained (Photo 32). It consists mainly of chlorite (or serpentine)-rich phyllosillicates with variable amounts of carbonates, magnetite, apatite, and pyrrhotite.

5.3. Anhydrous chondritic fragments

These fragments are up to several tens of microns across and seem to be fragments of chondrules or chondrites (Photos 33, 34, 35, and 36). They consist of olivine, pyroxene, sodic plagioclase, chromite, whitlockite, and troilite. They are free from hydrous minerals.

6. Mineralogy

6.1. Phyllosilicates

Phyllosilicates in non-Antarctic CI chondrites occur as main constituents and they are serpentine and smectite (TOMEOKA and BUSECK, 1988). The smectite group in terrestrial samples stands for dioctahedral and trioctahedral phyllosilicates having a talc structure. It includes small amounts of Al, ferric Fe, alkalis, and Ca. The CaO contents are usually higher than the alkali contents in the terrestrial smectite group. The phyllosilicates in Y-82162 contain higher alkali contents than CaO, and the term "sodian talc" which was introduced by SCHREYER *et al.* (1980) is used instead of smectite; the talc, $Mg_6Si_8O_{20}(OH)_4$, forms a solid solution to sodium-aluminum talc, $NaMg_6(Si_7Al)(OH)_4$. Here I use "sodian talc" for the alkali-rich half of the solid solution between sodium-free talc and sodium-aluminum talc (Fig. 1b). In Fig. 1a, the compositional range of sodian talc is shown, where sodium-ferric iron talc, $NaMg_6(Si_7Fe^{3+})O_{20}(OH)_4$, is also shown.

Representative chemical compositions of phyllosilicates in each clast-type are shown in Table 3.

6.1.1. Phyllosilicates in the matrix

The composition of phyllosilicates in the matrix (Table 3) shows that the total wt% of the major element oxides is about 80% and that most of the rest may be water. In Fig. 1, chemical compositions of phyllosilicates in the matrix are plotted; they form

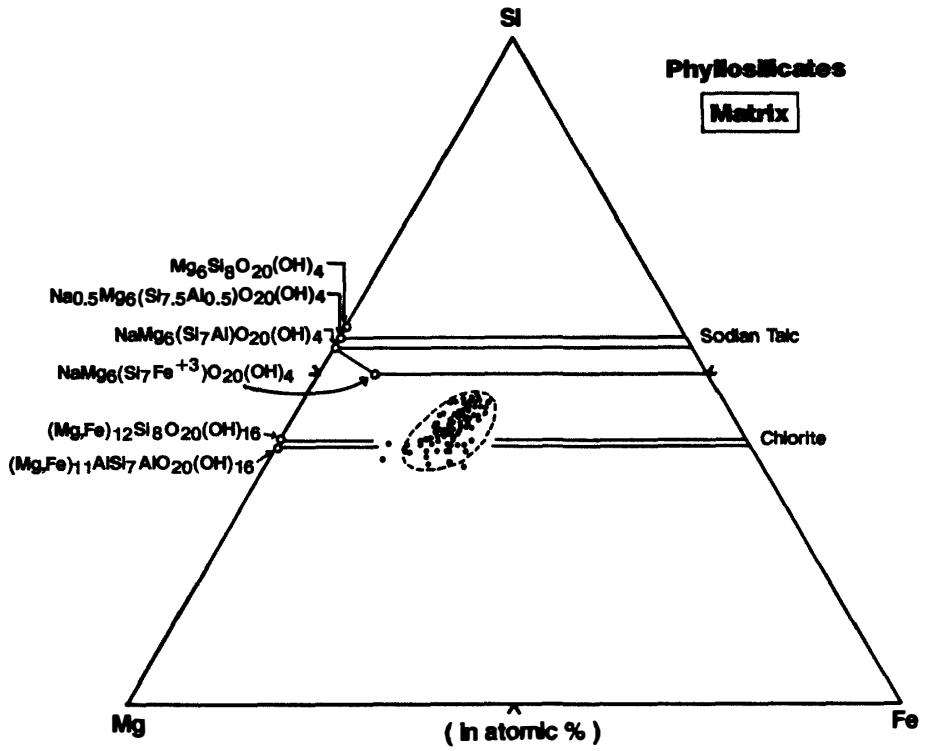

Fig. 1a. Chemical compositions of phyllosilicates in the matrix. Stoichiometric compositions of talc, sodium-aluminum talc, intermediate talc between the former two, sodium-ferric iron talc, antigorite, and aluminous chlorite are shown for reference. Note that the matrix phyllosilicates form a tight cluster.

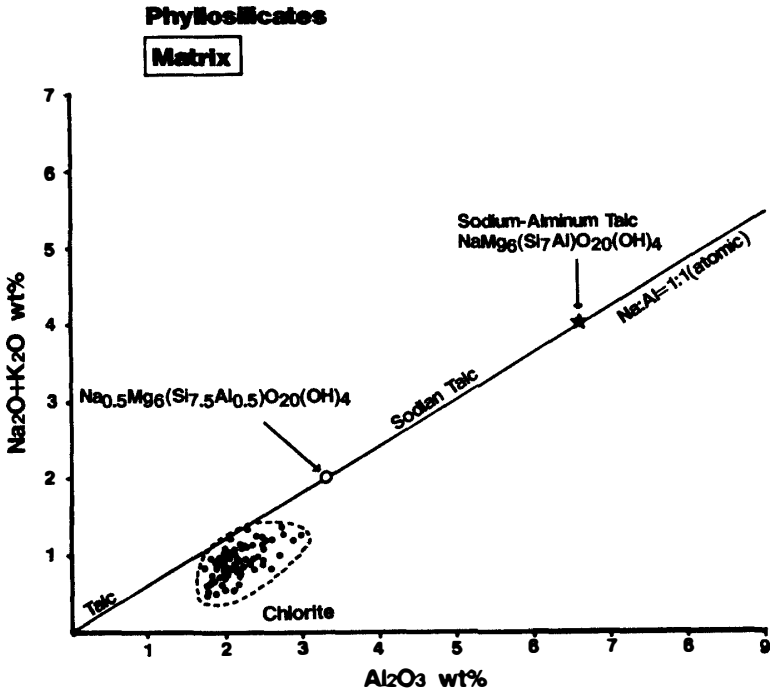

Fig. 1b. Chemical compositions of phyllosilicates in the matrix. They are chlorite (or serpentine)*-rich phyllosi-licates.*

Table 3. Representative chemical compositions of sodian talc-rich and chlorite-rich phyllosilicates in sodian talc-rich (Sod-Talc), chlorite-rich (Chlorite), magnetite, apatite-rich chlorite-rich (Ap-rich), CaO-rich unusual (Unusual), and composite (Comosite-reac. zone, reaction zone between sodian talc-rich phyllosilicates and magnetites) clasts and the matrix.

	Sod-Talc clasts		Chlorite clasts	Magnetite clasts	Ap-rich clasts	Unusual clasts	Composite reac. zone	Matrix
	S-Talc	S-Talc	Chl	Chl	Chl	MnO-Chl	Chl	Chl
SiO_2	51.20	47.08	40.57	37.04	40.20	37.43	37.95	34.59
TiO_2	0.00	0.00	0.12	0.00	0.00	0.00	0.03	0.07
Al_2O_3	5.88	5.06	2.02	3.31	2.56	3.22	2.88	2.03
Cr_2O_3	0.00	0.25	0.13	1.51	0.82	1.31	0.77	0.57
FeO	7.56	9.73	21.56	22.27	16.14	24.07	22.37	21.17
MnO	0.00	0.00	0.19	0.83	0.07	4.87	0.20	0.21
MgO	26.52	27.51	18.89	23.86	22.95	20.58	27.56	20.46
CaO	0.00	0.02	0.10	0.33	0.34	0.33	0.07	0.24
Na_2O	4.15	4.35	0.88	1.27	1.28	1.21	0.70	0.58
K_2O	0.29	0.23	0.09	0.09	0.08	0.06	0.21	0.27
Total	95.60	94.23	85.55	90.51	84.44	93.08	92.74	80.19

* All Fe as FeO. S-Talc and Chl are sodian talc-rich and chlorite (or serpentine)-rich phyllosilicates.

a tight cluster. Figure 1a suggests that the phyllosilicates are mainly chlorite or serpentine with a subordinate amount of sodian talc. The high alumina contents ranging from 1.5 to 3 wt% and high alkali (Na_2O+K_2O) contents ranging from 0.5 to 1.5 wt% (Fig. 1b) suggest that the main phyllosilicates are mixtures of chlorite or serpentine with a subordinate amount of sodian talc. The two kinds of phyllosilicates

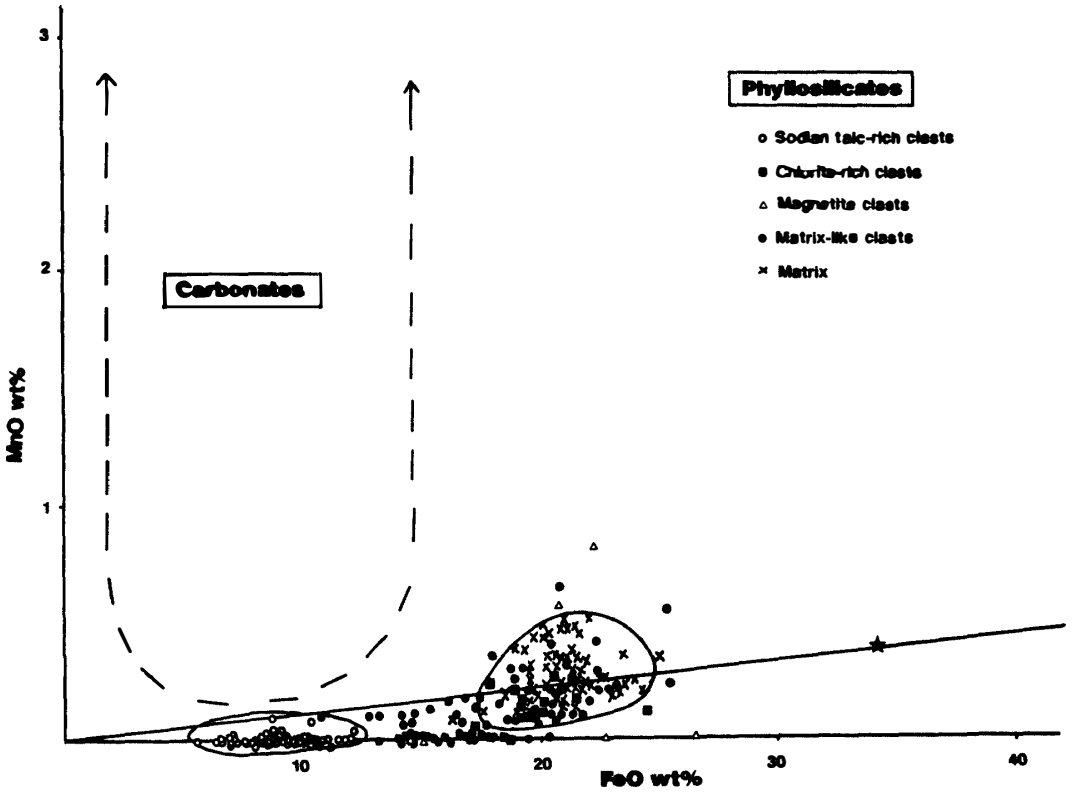

Fig. 2a. The MnO contents of phyllosilicates in Y-82162 are plotted against the FeO contents (all Fe as FeO). The compositional range of carbonates is shown for reference. Note that the Mn/Fe ratios of phyllosilicates in sodian talc-rich clasts are very low.

may occur as mixed layers (SCHREYER *et al.*, 1980) or as individual tiny grains. Their Mg/(Mg+Fe) atomic ratios range from 0.55 to 0.73 (Fig. 1a) with the average of 0.64. Figure 2a shows that the MnO contents of the matrix phyllosilicates range from 0.1 to 0.5 wt% but the average value of Mn/Fe atomic ratios is similar to that of the solar system elemental abundance. The Cr_2O_3 contents range from 0.4 to 0.8 wt%, forming a tight cluster in Fig. 2b.

6.1.2. Phyllosilicates in phyllosilicate clasts

In Fig. 3a, phyllosilicates in sodian talc-rich clasts form a tight cluster and are different from the compositional range of the matrix phyllosilicates. Figure 3b shows that phyllosilicates in the sodian talc-rich clasts contain high concentrations of alkalis ranging from 2 to 5.5 wt% and deviate from the solid solution line between sodium-free talc and sodium-aluminum talc. The deviation may be due to the substitution of Si and/or 2Mg by $NaFe^{3+}$. Their compositions suggest that the phyllosilicates in sodian talc-rich clasts are mainly sodian talc including ferric irons with a subordinate amount of a chlorite (or serpentine) component. Their Mg/(Mg+Fe) atomic ratios range from 0.79 to 0.89 (Fig. 3a) with the average value of 0.84. The MnO and CaO contents of sodian talc-rich phyllosilicates are less than 0.1 wt% (Table 3), and their MnO/FeO ratios (all Fe as FeO) are very low (Fig. 2a). Their Cr_2O_3 wt% range from zero up to 2 wt% (Fig. 2b).

On the other hand, phyllosilicates in chlorite-rich clasts are different in chemical

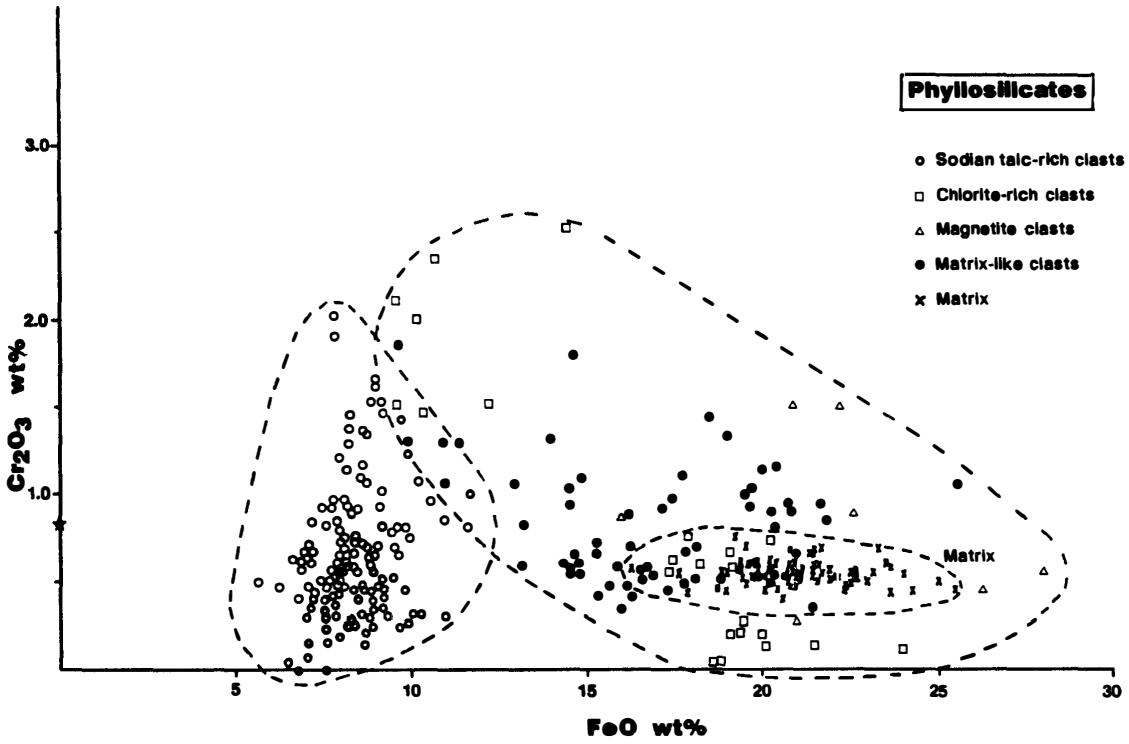

Fig. 2b. The Cr_2O_3 contents of phyllosilicates in Y-82162 are plotted agaist the FeO contents (all Fe as FeO).

compositions from those in sodian talc-rich clasts, being SiO_2-poorer and FeO-richer than the latter (Fig. 3a). They are intermediate in chemical composition between phyllosilicates in the matrix and sodian talc-rich clasts, and mainly chlorites with subordinate amounts of sodian talc components (Fig. 3). Their Mg/(Mg+Fe) atomic ratios range from 0.60 to 0.86. Their MnO contents are less than 0.3 wt% (Fig. 2a), and Cr_2O_3 contents range from zero up to 2.5 wt% (Fig. 2b).

6.1.3. Phylloslilicates in matrix-like clasts

Phyllosilicates in matrix-like clasts occur as microspherules, networks, vein-filling minerals, and fine-grained massive aggregates, and their compositions are separately plotted in Fig. 4. The phyllosilicates within microspherules and of networks are similar in chemical composition to each other, but they are slightly richer in MgO and Al_2O_3 than fine-grained massive aggregates. The compositional range of phyllosilicates in veins coincides with alkali-poor portion of ther ange of phyllosilicates in sodian talc-rich clasts (Fig. 4b), but vein phyllosilicates which cut directly magnetite grains are FeO-rich chlorites. The massive phyllosilicates in matrix-like clasts are similar to those in chlorite-rich clasts and the matrix, although some deviate from the compositional ranges of the latter. Their MnO and Cr_2O_3 contents are similar to those of chlorite-rich clasts (Fig. 2).

6.1.4. Phyllosilicates in unusual clasts

Phyllosilicates occur in one CaO-rich unusual clast including abundant magnetites (Photo 15). The representative composition of the phyllosilicates (Table 3) shows that they are rich in FeO and MnO contents. The MnO content is remarkably high,

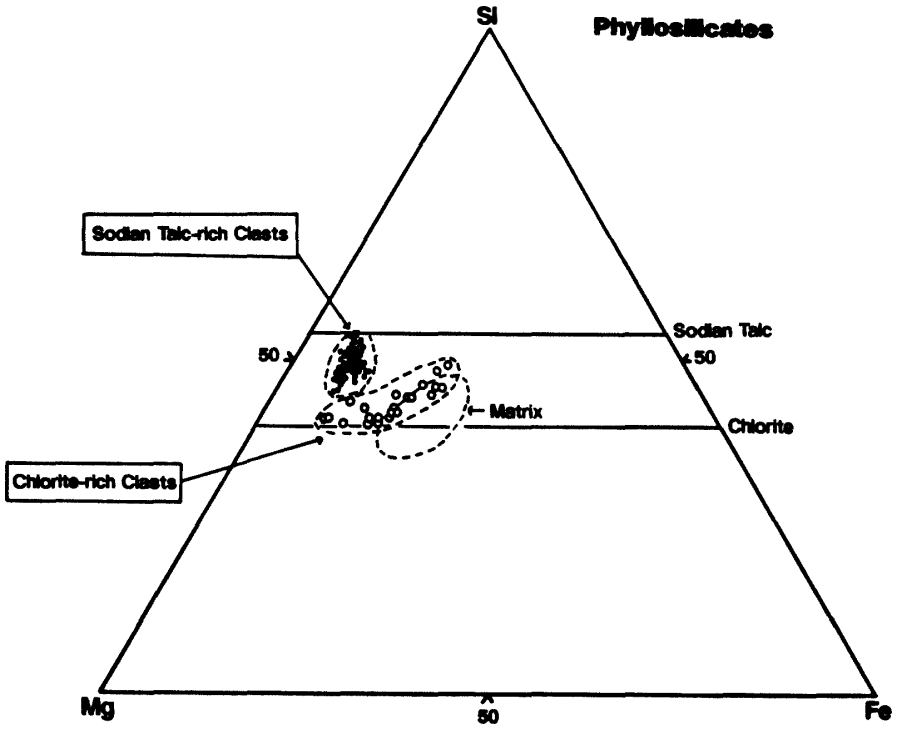

Fig. 3a. Chemical compositions (in atomic %) of phyllosilicates in 13 sodian talc-rich clasts (solid circles) and 4 chlorite-rich clasts (open circles). Note that sodian talc-rich phyllosilicates in sodian talc-rich clasts form a tight cluster.

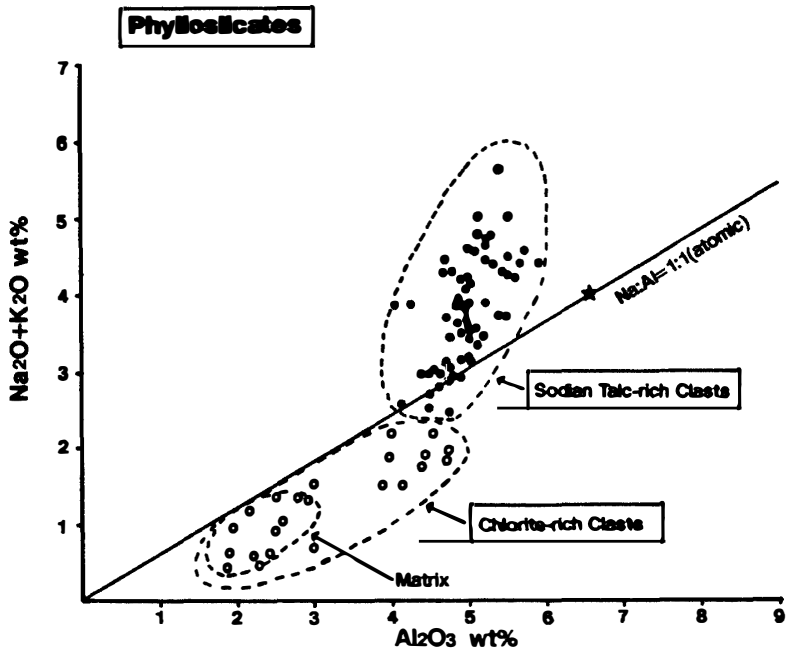

Fig. 3b. Chemical compositions of phyllosilicates in 13 sodian talc-rich clasts (solid circles) and 4 chlorite-rich clasts (open circles). A solid star on the straight line is stoichiometric sodium-aluminum talc.

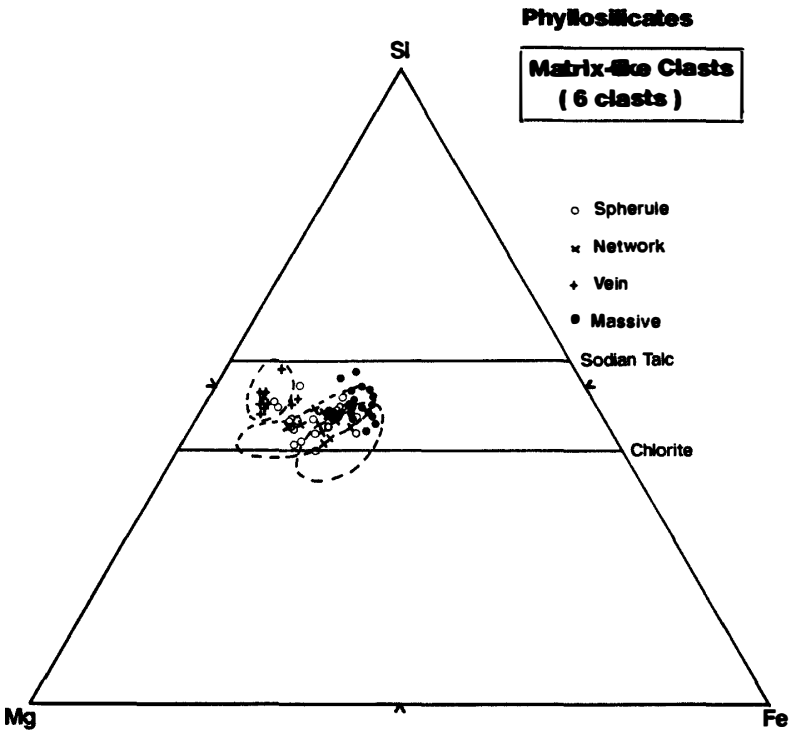

Fig. 4a. Chemical compositions (in atomic %) of phyllosilicates in 6 matrix-like clasts. Note that vein phyllosilicates are plotted in the range of sodian talc-rich clast-type, and that the other phyllosilicates are plotted in the range of chlorite-rich clast-type.

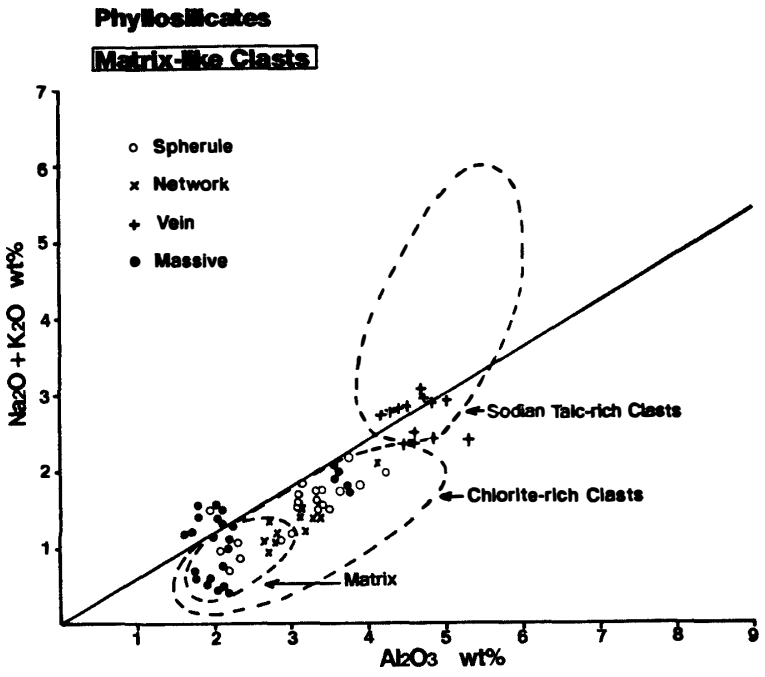

Fig. 4b. Chemical compositions of phyllosilicates in 6 matrix-like clasts.

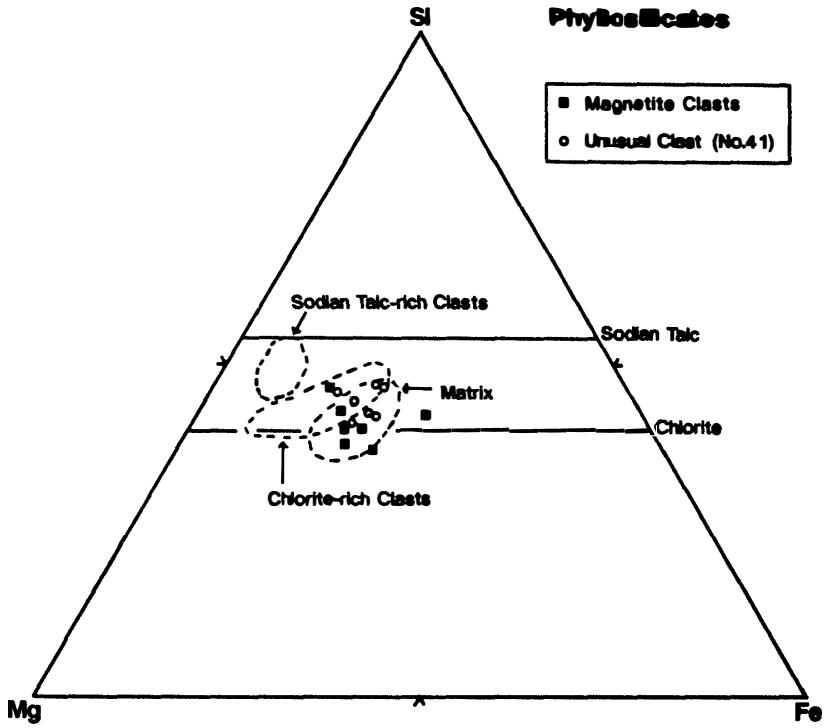

Fig. 5a. Chemical compositions (in atomic %) of phyllosilicates in 4 magnetite clasts and one unique clast (No. 41) of CaO-rich unusual clasts. Note that the phyllosilicates in magnetite clasts are richer in Fe than those of chlorite-rich clast-type.

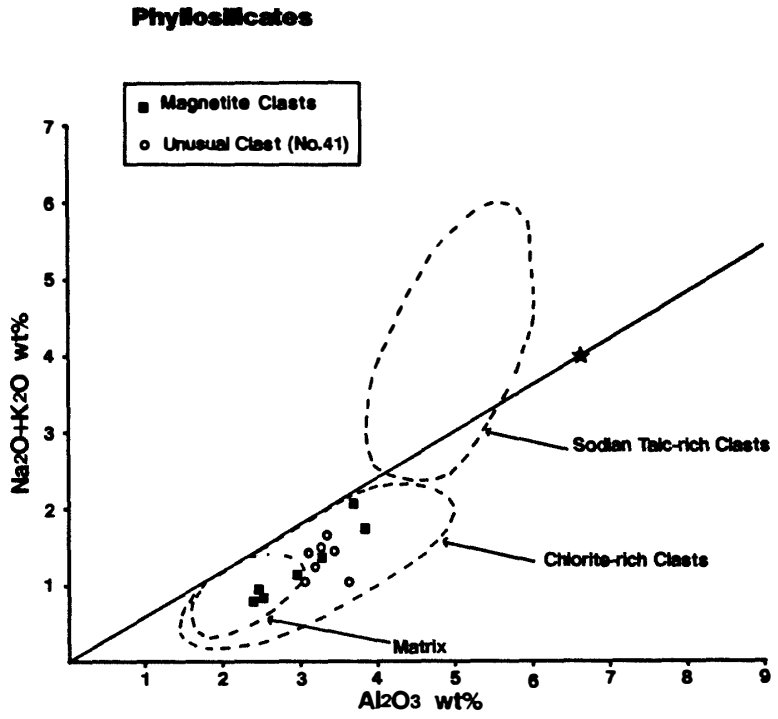

Fig. 5b. Chemical compositions of phyllosilicates in 4 magnetite clasts and one unique clast (No. 41) of CaO-rich unusual clast-type. Note that the phyllosilicates in magnetite clasts are plotted in the range of the chlorite-rich clast-type.

ranging from 4 to 5 wt%. Figure 5 indicates that the phyllosilicates are mainly chlorite and similar in chemical composition except for the high MnO content to those in magnetite clasts.

6.1.5. Phyllosilicates in magnetite clasts

As shown in Fig. 5a, phyllosilicates in magnetite clasts are mainly chlorites richer in Fe than those in chlorite-rich clasts and similar to those in the matrix. However, Fig. 5b indicates that the phyllosilicates are similar in alkali and alumina contents to those in chlorite-rich clasts. Their MnO and Cr_2O_3 contents also are similar to those of phyllosilicates in chlorite-rich clasts (Fig. 2).

6.1.6. Phyllosilicates in composite clasts

The chemcial compositions of phyllosilicates in composite clasts are plotted in Fig. 6. Their chemical compositions coincide with the compositional ranges of phyllosilicates in all clast-types. This is the natural consequence derived from the definition. However, phyllosilicates which are directly in contact with magnetite in composite clasts are enriched in Fe within a few tens of microns in width (Photos 24 and 25), and the Mg/(Mg+Fe) atomic ratios range from 0.60 to 0.73 (Fig. 6a and Table 3).

6.2. Carbonates

Carbonates in each clast-type are similar in chemical composition to each other and most of them are very fine-grained aggregates. They contain variable amounts of SiO_2 ranging from zero to more than 10 wt%, concentrating in a range from 3 to

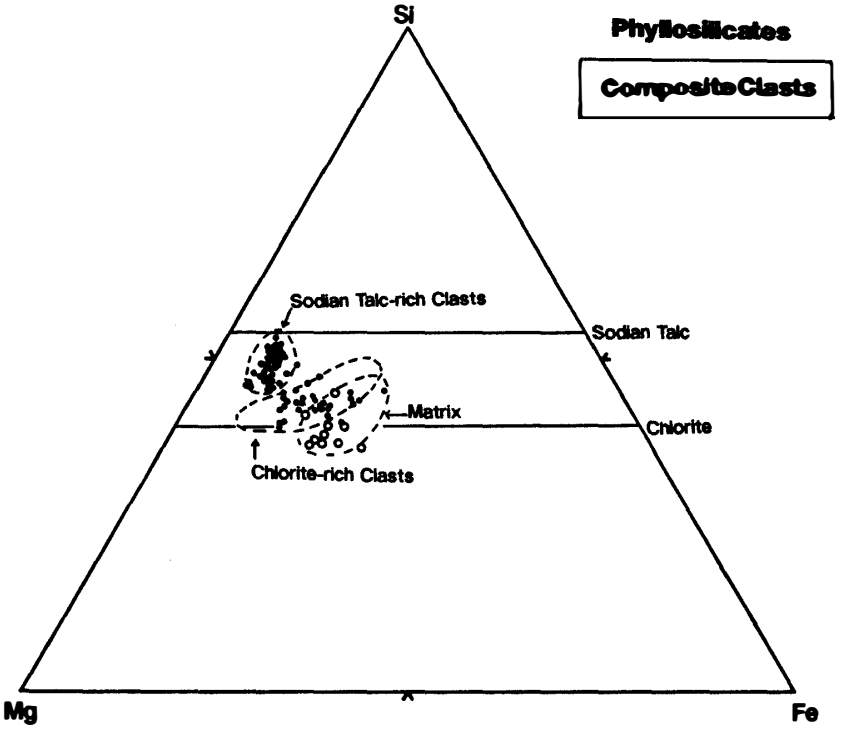

Fig. 6a. Chemical compositions (in atomic %) of phyllosilicates in 8 composite clasts (solid circles). Open circles are phyllosilicates which are directly in contact with magnetite grains, which become Fe-rich.

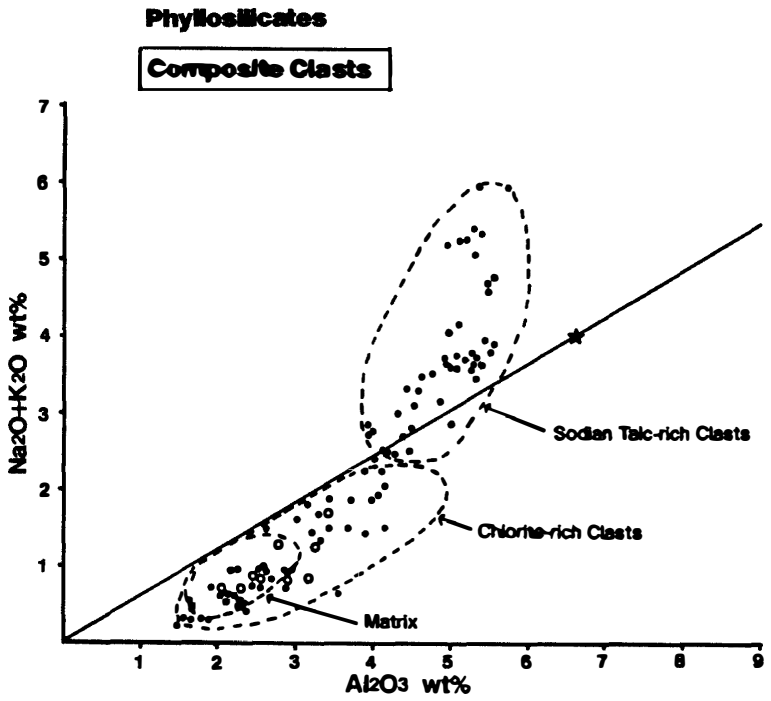

Fig. 6b. Chemical compositions of phyllosilicates in 8 composite clasts. Symboles are the same as those in Fig. 6a.

Table 4. Representative chemical compositions of carbonate aggregates in phyllosilicate (Phyl), carbonate (Carb), and unusual (Unus) clasts. Ank, Dol, and Rho are mainly ankerite, dolomite and rhodochrosite, respectively.

	Phyl Ank	Carb Ank	Carb Dol	Unus Ank	Unus Rho
SiO_2*	6.61	3.28	1.69	5.79	0.00
TiO_2	0.00	0.00	0.00	0.00	0.00
Al_2O_3	0.00	0.04	0.09	0.02	0.00
Cr_2O_3	0.00	0.00	0.00	0.00	0.02
FeO	11.28	9.02	2.61	9.51	7.25
MnO	2.78	0.67	0.24	0.61	44.91
MgO	13.35	5.15	16.33	5.38	10.86
CaO	22.80	36.18	28.39	34.72	0.94
Na_2O	0.16	0.84	0.66	0.36	1.92
K_2O	0.00	0.00	0.00	0.00	0.03
Total**	56.98	55.18	50.01	56.39	65.43

* Small amounts of silica minerals or amorphous silica may be included in the carbonate aggregates.
** The CO_2 contents are not determined.

7 wt% with an average of about 5 wt%. The high silica contents may be due to submicroscopic silica minerals or amorphous silica which are included among carbonate grains. Representative chemical compositions are shown in Table 4.

Chemical compositions of carbonates in carbonate clasts are plotted in Fig. 7. Most carbonates are ankerites which are distributed parallel to the Ca-Mg join of the figure, meaning that siderite components are nearly constant at a range from 10 to 25 mol %. Most carbonate clasts have a dolomite rim, and the dolomites are poorer

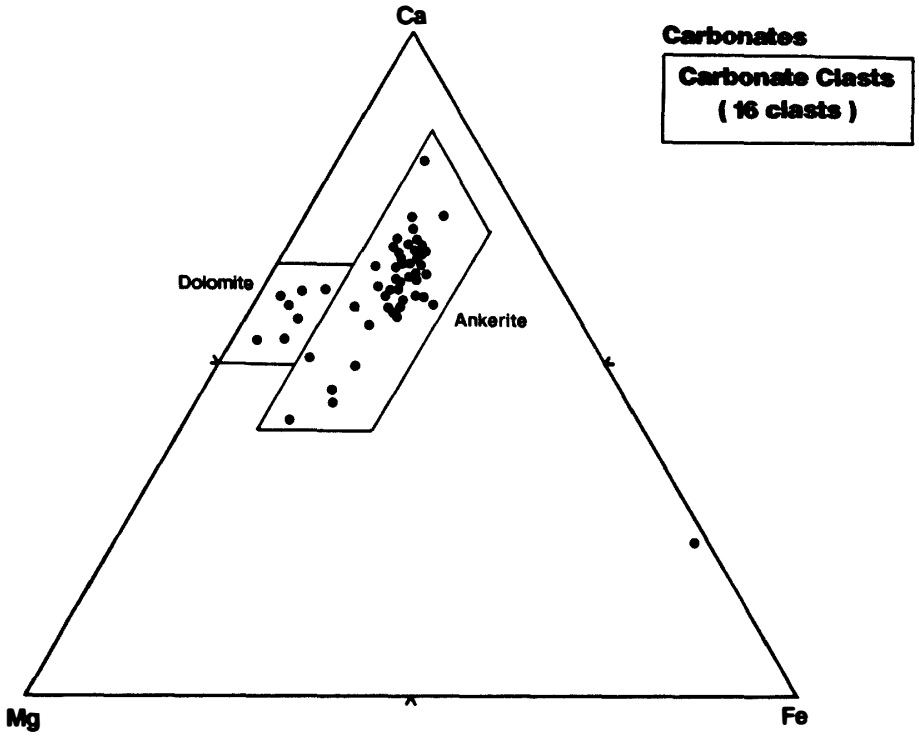

Fig. 7. Chemical compositions (in atomic %) of carbonates in 16 carbonate clasts. The main carbonates are ankerites with the range of Fe/(Ca+Mg+Fe) atomic ratios from 0.10 to 0.25, and the ratios of thin dolomite rims are less than 0.10.

in siderite components in comparison to the ankerites and form a tight compositional cluster in Fig. 7. The MnO contents of most carbonates range widely from 0.2 wt% to 9 wt% (Fig. 2a).

Carbonates in CaO-rich unusual clasts occur as mantles or outermost rims. The mantles are mainly ankerites similar in chemical compositions to those in carbonate clasts. The outermost rims are dolomites similar to those of the rims of carbonate clasts. Minor amounts of carbonates occur in the oxide cores of CaO-rich unusual clasts, and they will be discussed in the following Section 6.3.

6.3. Oxides and oxide-carbonate aggregates

Oxides in Y-82162 are magnetite, periclase, and ilmenite. Chromites are found in an anhydrous chondritic fragment and will be discussed in the Section 6.6.

6.3.1. Magnetites

Magnetites occur in all clast-types except for sodian talc-rich clast-type. They show various textural types; framboidal aggregates, plaquettes, spherulites, and irregular or subrounded grains. However, there is no difference in chemical compositions among the textural types. Representative chemical compositions of magnetites are shown in Table 5, and all magnetites in each clast-type are shown in Fig. 8. Magnetites in chlorite-rich clasts and magnetite clasts are MnO-poor type with a concentration of less than 1.5 wt% MnO and 3.0 wt% MgO. On the other hand, those in carbonate clasts and unusual clasts are MnO-rich with a compositional range from 1.5

Table 5. Representative chemical compositions of magnetites (Mt) in phyllosilicate (Phyl), carbonate (Carb), unusual (Unus), magnetite (Mag), and composite (Comp) clasts, and an isolated ilmenite (Il) with chemical zoning from Mn-rich cores to Mn-poor rims.

	Phyl Mt	Carb Mt	Unus Mt	Unus Mt	Mag Mt	Comp Mt	Il core	Il rim
SiO_2	0.00	0.18	0.00	0.00	0.00	0.00	0.00	0.13
TiO_2	0.00	0.00	0.00	0.00	0.00	0.00	52.75	52.74
Al_2O_3	0.00	0.00	0.00	0.05	0.00	0.00	0.02	0.00
Cr_2O_3	0.10	0.03	0.02	0.04	0.00	0.00	0.19	0.32
FeO	87.96	81.35	87.09	81.86	89.32	88.85	40.52	39.52
MnO	0.04	5.49	3.11	4.29	0.06	0.00	5.10	3.54
MgO	0.33	2.05	0.70	3.86	0.22	0.24	0.63	2.29
CaO	0.00	0.33	0.30	0.83	0.00	0.00	0.00	0.00
Na_2O	0.06	0.00	0.05	0.00	0.00	0.00	0.05	0.00
K_2O	0.00	0.00	0.00	0.00	0.00	0.00	0.00	0.02
Total	88.49	89.43	91.27	90.93	89.60	89.09	99.26	98.56

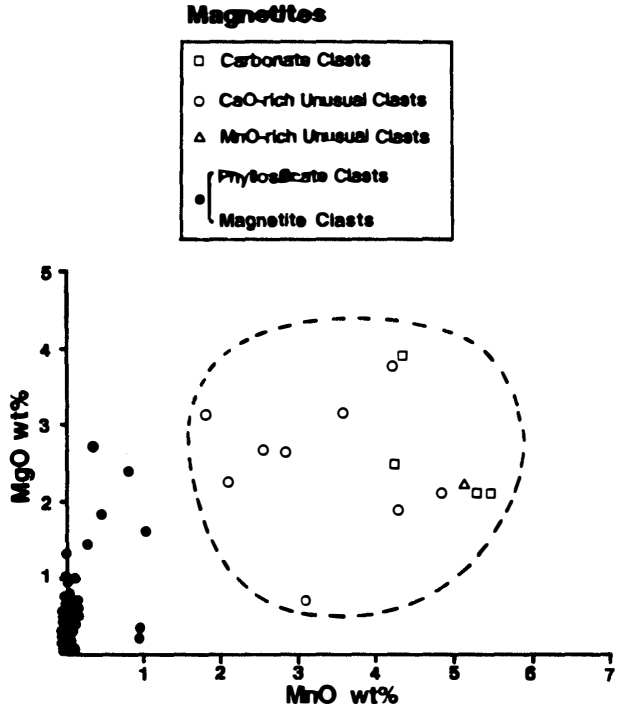

Fig. 8. Chemical compositions of magnetites in each clast-type. Note that they are divided into two groups, MnO-rich (open symbols) and MnO-poor (solid symbols) magnetites.

to 5.5 wt% of MnO and from 0.5 to 4.0 wt% of MgO.

6.3.2. Periclases and accompanying minerals

Periclase, an unknown Fe-Ca-S-O phase (alpha phase), and fine-grained aggregates (PCA aggregate) occur in the cores of CaO-rich unusual clasts with minor and variable amounts of pyrrhotite, magnetite, and apatite. Their compositions are shown in Table 6 and in Fig. 9a. The periclases are FeO-bearing ones with MgO/(MgO+FeO) rations ranging from 0.75 to 0.55. They are rich in MnO ranging from 6.2 to 7.2 wt%, and are poor in CaO ranging from 0.3 to 1.1 wt%. The chemical com-

positions of alpha phase are shown in Fig. 9a and seem to be contaminated by the neighboring periclase grains during the EPMA analyses. The contamination-free composition is tabulated in Table 6, showing that the alpha phase is an unknown

Table 6. Chemical compositions (wt %) of periclase, alpha phase, PCA-, PER-, and PMN-aggregates in unusual clasts.

	CaO-rich unusual clast			MnO-rich unusual clast	
	Periclase	Alpha	PCA	PER	PMN
Mg	31.09	0.56	16.36	29.08	20.43
Ca	0.44	21.89	15.75	0.33	1.43
Mn	5.08	0.52	2.36	3.22	19.06
Fe	32.56	41.11	10.86	24.87	13.06
Ni	0.00	0.00	—	0.08	0.13
O	31.68	13.62	31.87	27.53	34.35
S	0.00	19.72	0.47	0.56	3.76
P	0.00	1.68	—	0.00	0.00
Total	100.85	99.10	77.67	85.67	92.22
	↑	↑	↑	↑	↑
	$(Mg_{0.67}Fe_{0.33})O$	$15FeS \cdot 13CaO \cdot 3FeO$	$20MgO \cdot 6FeO + 12CaCO_3$	$35MgO \cdot 12FeO + FeS$	$23MgO \cdot 3FeO + 10MnCO_3 + 3FeS$

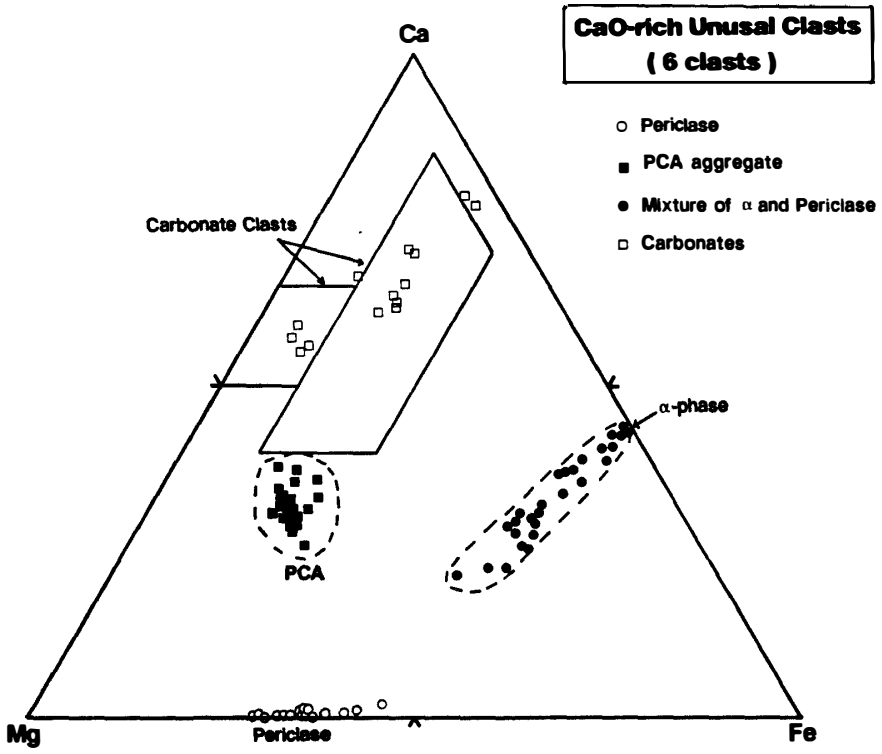

Fig. 9a. Chemical compositions (in atomic %) of periclase, alpha phase, PCA aggregate, and carbonates in 6 CaO-rich unusual clasts. Note that alpha phase is nearly free of MgO. MgO-bearing alpha phase may be contaminated by the neighboring periclase during the EPMA analyses.

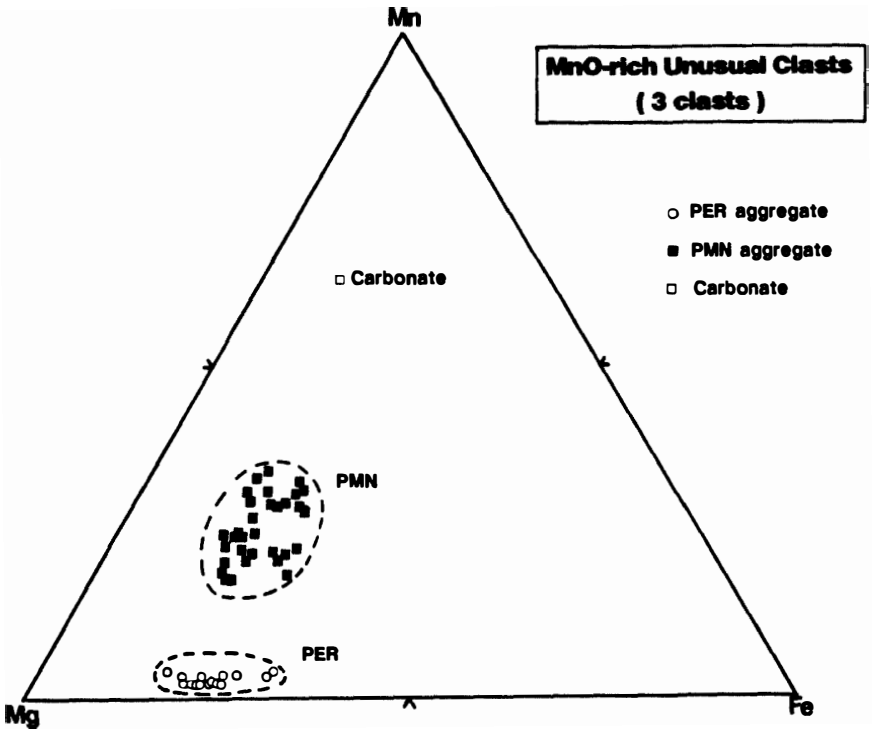

Fig. 9b. Chemical compositions (in atomic %) of PER aggregate, PMN aggregate, and carbonates of PMN aggregate in the MnO-rich subtype of CaO-poor unusual clasts.

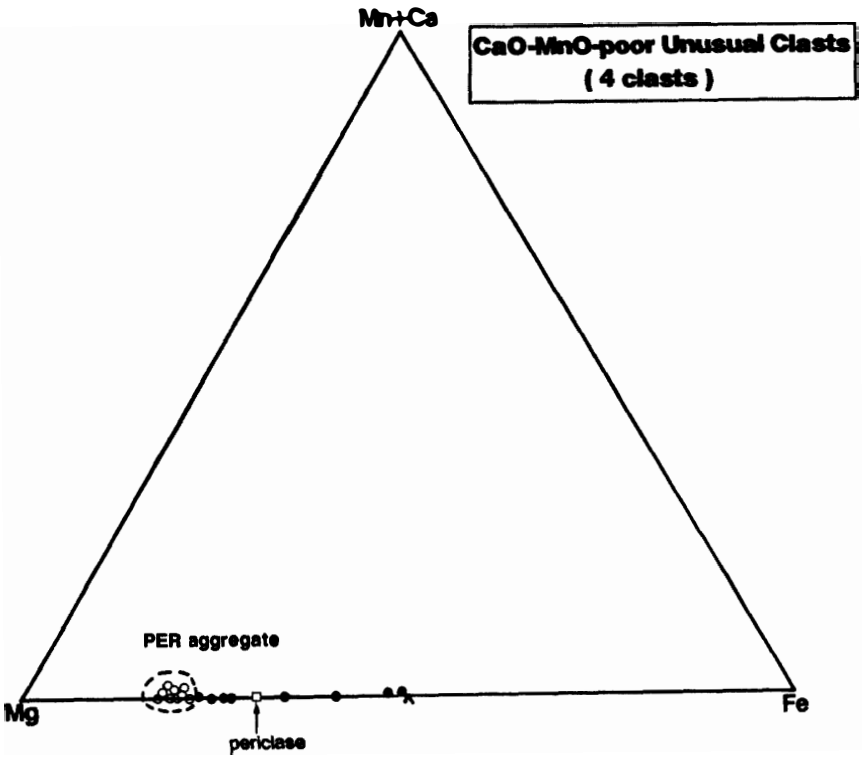

Fig. 9c. Chemical compositions (in atomic %) of PER aggregate (open circles), periclase (open square), and FeS-bearing fine-grained aggregates (solid circles) in the MnO-poor subtype of CaO-poor unusual clasts.

mineral consisting of Fe monosulfide and Ca-Fe oxide components in nearly equal amounts with a minor P_2O_5 component. The PCA aggregate is very fine-grained, and each grain is too small to be analyzed. The chemical compositions of the PCA aggregate obtained by a focussed beam of an EPMA give low total wt% of 75–80 (Table 6) but form a cluster in Fig. 9a. The low total wt% may be partly due to the fine grain sizes and partly due to the carbon content. The PCA aggregate consists mainly of FeO-bearing periclase and Ca-carbonate (Table 6).

The Mn-rich type of CaO-poor unusual clasts consists mainly of two kinds of fine-grained aggregates (PER and PMN aggregates), and their compositions are shown in Fig. 9b, forming two separate clusters. The representative chemical compositions are shown in Table 6, indicating that the PER aggregate consists mainly of FeO-bearing periclase with a minor amount of FeS. The PMN aggregate consists of FeO-bearing periclase, Mn-rich carbonates and FeS. The Mn-rich carbonate may be rhodochrosite (Table 6), and the chemical composition of a rhodochrosite grain, which is large enough to be analyzed, is shown in Table 4.

The MnO-poor type of CaO-poor unusual clasts consists of fine-grained PER aggregates with a minor amount of FeS. Their compositions are shown in Fig. 9c, indicating that the PER aggregate is homogeneous in MgO/(MgO+FeO) with the ratio of about 0.80, although FeS-rich aggregates (S content more than 1 wt%) show the wide range of the ratio. One periclase grain in a clast is large enough to be analyzed, and the MgO/(MgO+FeO) ratio is 0.7 (MgO=43.57, MnO=0.11, and MgO=55.83 wt%).

6.3.3. Ilmenite

Ilmenite occurs as an isolated mineral in matrix-like clasts and the representative chemical composition is shown in Table 5. It is zoned; the core is about 5.5 wt% MnO and 0.5 wt% MgO, whereas about 3.5 wt% MnO and 2.5 wt% MgO were analyzed in the rim. The atomic ratios of (Fe+Mn+Mg)/Ti are nearly one, suggesting that the ilmenites are free of hematite component.

6.4. Phosphates

Phosphates in Y-82162 are apatites except for those in anhydrous chondritic fragments. The representative chemical compositions are shown in Table 7. They are nearly stoichiometric in composition with the formula, $Ca_5(PO_4)_3 \cdot (OH, F)$. The F contents are variable, grain by grain, and range from zero to 3 wt%.

6.5. Sulfides, metals, and hydroxides

Pyrrhotite, pentlandite, chalcopyrite, and awaruite are homogeneous in chemical composition in Y-82162, and the representative compositions are shown in Table 8. Awaruite contains high Co content of about 2 wt%, and the Ni/(Ni+Fe) atomic ratio is about 0.70. Pyrrhotites are low in Ni and Co contents, and the Fe/S atomic ratios are nearly one. Pentlandite contains high Co content of about 1.2–1.5 wt%. The Ni/(Ni+Fe) atomic ratios are about 0.33, and the (Fe+Ni+Co)/S atomic ratios are nearly one. Chalcopyrite is free of Ni and Co, and the chemical formula is $Cu_3Fe_4S_7$.

Ferrihydrite occurs at the rim of pyrrhotite grains and are nearly free of Ni and

Table 7. Representative chemical compositions of apatites (Ap) in chlorite-rich clasts (Chl) and composite clasts (Comp).

	Chl Ap	Chl Ap	Chl Ap	Comp Ap
FeO	0.16	0.58	0.27	0.64
MnO	0.55	0.67	0.04	0.49
MgO	0.16	0.12	0.06	0.30
CaO	54.94	55.13	56.48	56.27
Na_2O	0.00	0.22	0.22	0.00
K_2O	0.09	0.00	0.00	0.00
P_2O_5	40.95	41.35	41.79	41.42
Cl	0.00	0.00	0.00	0.32
F	2.50	1.68	1.27	0.00
−O*	−1.05	−0.71	−0.53	−0.07
Total	98.30	99.04	99.60	99.37

* The oxygen contents equivalent to Cl and F are shown by −O.

Table 8. Chemical compositions (wt%) of metals, sulfides, and hydroxides in the Y-82162 chondrite. Below the table, stoichiometric compositions are shown.

	Awaruite	Pyrrhotite	Pentlandite	Chalcopyrite	Ferrihydrite
Fe	28.99	62.15	42.03	34.73	53.86
Co	1.97	0.04	1.25	0.01	—
Ni	67.53	0.17	21.67	0.03	0.19
Cu	0.00	0.01	0.22	30.16	—
Cr	0.00	0.05	0.06	0.00	—
Mn	0.00	0.00	0.00	0.23	0.00
S	0.04	37.00	33.84	34.93	14.60
O					O 26.61
Mg					Mg 1.35
Ca					Ca 0.87
Total	98.53	99.42	99.07	100.09	97.48
	↑	↑	↑	↑	↑
	$Ni_{69}Fe_{31}$	FeS	$(Fe_{0.67}Ni_{0.33})$ S	$Cu_3Fe_4S_7$	$15FeS \cdot 15Fe(OH)_3$

Co, but it contains small amounts of Mg and Ca (Table 8). The chemical formula is nearly $15FeS \cdot 15Fe(OH)_3$.

6.6. Minerals in anhydrous chondritic fragments

As anhydrous chondritic fragments seem to have an different origin from the other constituent units of Y-82162 (see Section 7.1), the mineralogy of anhydrous chondritic fragments is separately presented in this section.

Representative chemical compositions of minerals in some anhydrous chondritic fragments are shown in Table 9, and pyroxenes and olivines are plotted in Fig. 10. Zoned olivines in an anhydrous chondritic fragment (Photo 33) range in composition from $Fo_{81}La_{0.1}$ to $Fo_{22}La_2$ (La: Ca_2SiO_4), suggesting that this is a fragment of a zoned-olivine chondrule. Fassaite in an anhydrous chondritic fragment (Photo 34) contains a high Al_2O_3 content up to 11.5 wt%, but is poor in TiO_2.

Orthopyroxenes in an anhydrous chondritic fragment (Photo 35) are homogeneous in chemical composition with MgO/(MgO+FeO) ratios of 0.15–0.16, and

Table 9. Representative chemcial compositions of minerals in three anhydrous chondritic fragments (Fragment Nos. 56, J-3, and 57). Ol, Px, Aug, and Fas are olivine, low-Ca pyroxene, augite, and fassaite, respectively.

	No. 56 Ol	No. 56 Px	No. 56 Aug	J-3 Ol	J-3 Px	J-3 Px	J-3 Px	J-3 Fas	No. 57 Ol	No. 57 Ol
SiO_2	39.74	57.22	51.91	40.66	57.52	57.14	49.16	45.44	38.43	32.26
TiO_2	0.03	0.08	0.30	0.00	0.07	0.14	1.72	2.85	0.00	0.07
Al_2O_3	0.00	0.54	4.77	0.07	0.85	1.07	7.60	11.48	0.04	0.47
Cr_2O_3	0.49	0.63	2.27	0.20	0.73	0.99	1.43	1.78	0.41	0.17
FeO	6.65	2.75	3.75	5.84	2.43	3.51	2.92	1.86	19.04	50.92
MnO	0.41	0.13	0.35	0.54	0.00	0.46	0.62	0.52	0.00	0.54
MgO	51.25	37.47	19.38	51.82	36.65	35.46	23.96	17.10	41.55	13.27
CaO	0.18	0.45	17.67	0.27	0.39	1.48	10.80	18.06	0.12	0.96
Na_2O	0.00	0.00	0.31	0.00	0.00	0.00	0.05	0.00	0.03	0.11
K_2O	0.00	0.00	0.00	0.00	0.00	0.00	0.00	0.00	0.00	0.00
Total	98.75	99.27	100.71	99.40	98.64	100.25	98.26	99.09	99.62	98.77

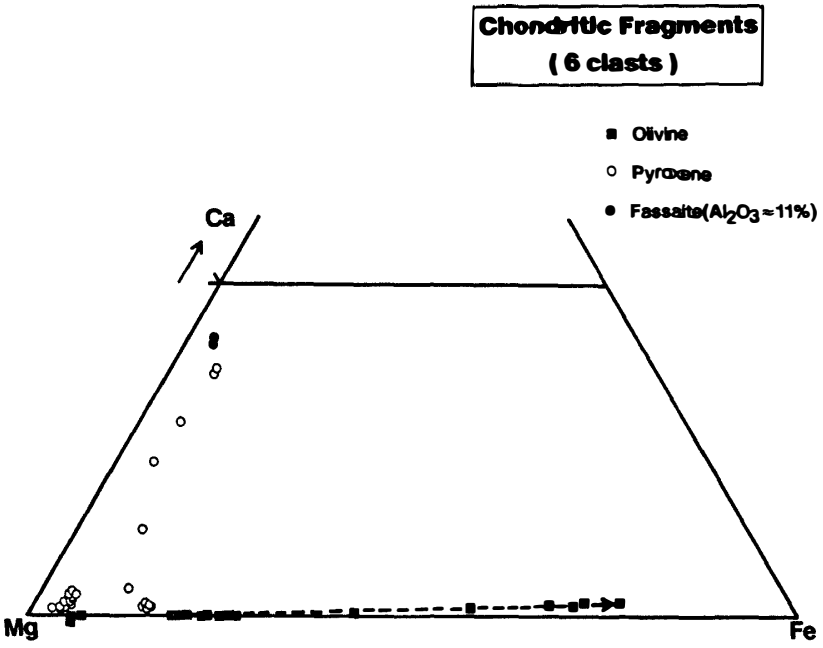

Fig. 10. Chemical compositions (in atomic %) of pyroxene and olivine in 6 anhydrous chondritic fragments. Anhydrous chondritic fragment (Photo 37) includes euhedral olivine grains showing a remarkable chemical zoning from magnesian cores to ferroan rims, which is shown by the dash-line with an arrow.

small plagioclase, chromite and whitlockite grains are included in the pyroxene. The plagioclase is oligoclase (An_{16}), and the chemical composition of chromite coincides with those of chromites in equilibrated H chondrites.

7. Discussion

7.1. Genetical relationship among clast types

The genetical relationships among all clast-types, matrix, and anhydrous chondritic

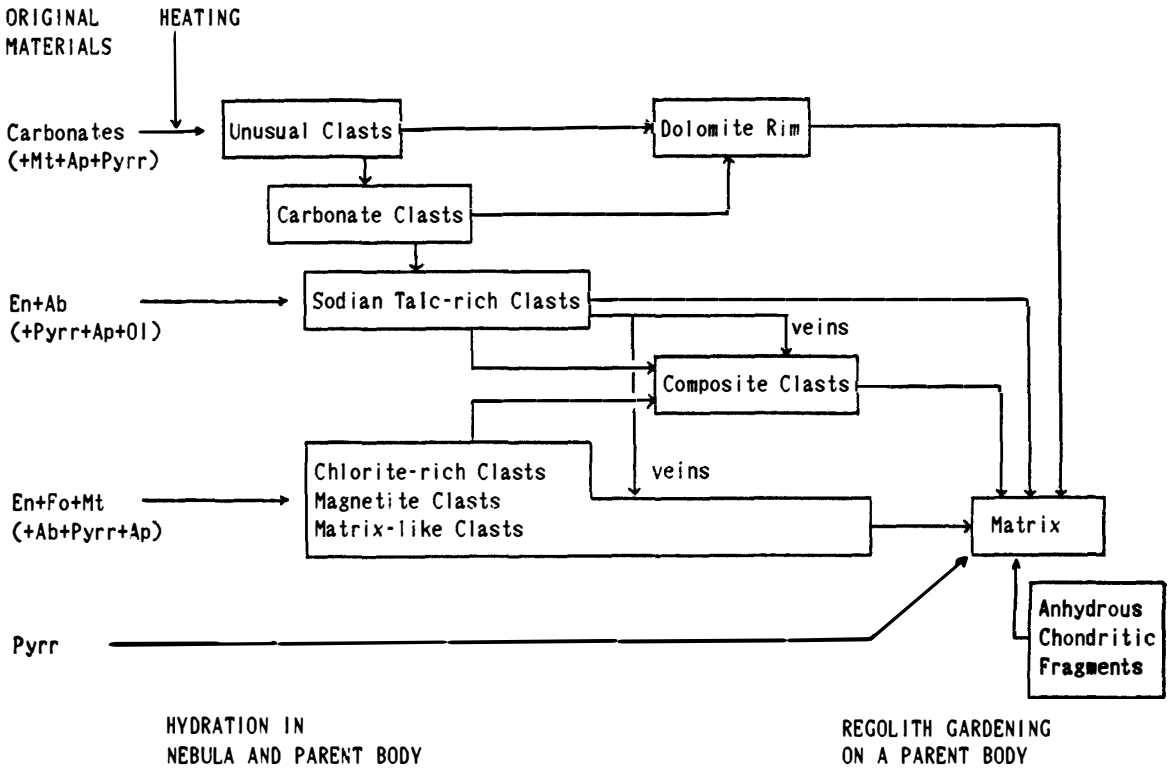

Fig. 11. Genetical relationships among clast-types in Y-82162. Mt, Ap, Pyrr, En, Ab, Ol, and Fo are magnetite, apatite, pyrrhotite, enstatite, albitic plagioclase, olivine, and forsterite, respectively.

fragments are schematically shown in Fig. 11 and discussed as follows.

As already stated in the Section 6.1, phyllosilicates which are directly in contact with magnetites are enriched in Fe in composite and matrix-like clasts, and this indicates that the phyllosilicates reacted with the neighboring magnetites to produce a FeO-rich chlorite component. A possible reaction is as follows;

$$\underset{\text{Talc}}{Mg_6Si_8O_{20}(OH)_4}+2\underset{\text{Mt}}{Fe_3O_4}+6H_2O\longrightarrow\underset{\text{Chl}}{Mg_6Fe_6Si_8O_{20}(OH)_{16}}+O_2\,, \qquad (1)$$

where Talc, Mt, and Chl are talc component in the phyllosilicate, magnetite, and ferroan chlorite (or serpentine) component, respectively. The FeO-rich chlorites directly in contact with magnetite have Mg/(Mg+Fe) ratios of 0.60–0.73 (Fig. 6a), and these values may be explained by the mixtures of ferroan chlorite produced by eq. (1) and magnesian chlorite (or serpentine) which existed in the original phyllosilicates. The FeO-rich chlorites are very similar in chemical composition to those in magnetite clasts, suggesting that FeO-rich chlorites in magnetite clasts were produced in a similar way to those in composite clasts.

The chlorites in some magnetite clasts show an amygdule texture which is similar to that in some chlorite-rich clasts, suggesting that chlorites in magnetite clasts were formed under similar conditions to those in chlorite-rich clasts. Phyllosilicates in matrix-like clasts except for those of the veins are similar in chemical composition to those in chlorite-rich clasts. Therefore, chlorite-rich, matrix-like and magnetite

clast-types may have formed under similar conditions (Fig. 11).

The occurrences of networks and microspherules of phyllosilicates in matrix-like clasts suggest that they were not produced in the nebula but in the parent body of Y-82162. Some matrix-like clasts are intruded by angular veins, and the veins seem to have formed in the cracks which were produced in the matrix-like clasts probably by impact events. In addition to this fact, the fine grain sizes of the phyllosilicates are similar to those of the matrix, and the matrix-like clast-type may have formed in a shallow level of the parent body.

Phyllosilicates of veins in matrix-like and composite clasts are similar in chemical composition to those in sodian talc-rich clasts, suggesting that the vein phyllosilicates were formed under similar conditions to those of sodian talc-rich clasts. Sodian talc-rich clasts and veins in matrix-like and composite clasts show well-crystallized textures in contrast to chlorite-rich and matrix-like clasts. The sodian talc-rich clasts may have been produced in hotter and deeper regions of the parent body, from fluidal phases, which assended into cracks in the matrix-like and composite clasts to produce the veins. The sodian talc-rich clasts are nearly free from magnetites, and the veins which directly cut magnetite grains in matrix-like and composite clasts became FeO-rich chlorites in the same way as eq. (1). These facts suggest that magnetite was unstable in a condition for the formation of sodian talc-rich clasts.

Carbonate clasts seem to have formed earlier than phyllosilicate clasts, because carbonate nodules, which are equivalent to the former, are included in the latter (Photo 1). Dolomite-rim-free carbonate clasts have sometimes a thin rim of sodian talc-rich phyllosilicates (Photo 11), and they may have been originally carbonate nodules which are observed in sodian talc-rich clasts. These nodules are never surrounded by dolomite rims, and the dolomite rims of dolomite-rimmed carbonate clasts may have been produced after the formation of phyllosilicate clasts (Fig. 11).

Unusual clasts include variable amounts of carbonates. CaO-rich unusual clasts have a structure of ankerite mantle and dolomite rim (Photo 12) similar in chemical composition to those of carbonate clasts. Therefore, the unusual clasts should have an intimate genetical relationship with carbonate clasts (Fig. 11).

Composite clasts consist of two or more clast-types, and they may have been formed in a latest stage of clast formation. In some composite clasts, reactions between magnetites and phyllosilicates took place to produce FeO-rich chlorites within a few tens of microns (Photo 24), suggesting that the formation temperature was high enough to react after the mixing of two or three clast-types.

Anhydrous chondritic fragments are very fresh and retain the original chemical zonation of the constituent minerals (Fig. 10). They have never experienced any hydration on the Y-82162 parent body, and must be projectiles which collided on the surface of the parent body to produce the regolith breccia of Y-82162 (Fig. 11). This is consistent with the fact that a fresh high-Al fassaite grain occurs in an anhydrous fragment (Photo 34), because high-Al fassaites are apt to decompose during alteration or metamorphic events (IKEDA, 1989). The chemical zoning and occurrence of olivine and pyroxene in some chondritic fragments are similar to those of some kinds of chondrules in unequilibrated chondrites, and such chondritic fragments may have been derived from unequilibrated chondrites. On the other hand, one fragment

(Photo 35) consists of homogeneous orthopyroxene, sodic plagioclase, chromite, and whitlockite, and these minerals are similar in chemical composition to those in equilibrated H chondrites. This fact suggests that this may be a fragment of equilibrated H chondrites, although kamacites, which are included abundantly in H chondrites, are not found in this fragment and in the matrix of Y-82162.

7.2. Formation of unusual clasts and carbonate clasts

The intimate genetical relationships between unusual and carbonate clast-types are suggested by the following reasons; (1) very fine-grained aggregates (PCA and PMN) in unsual clasts consist of Mg-Fe oxides and carbonates, (2) CaO-rich unusual clasts have an ankerite mantle and a dolomite rim similar to those of some carbonate clasts, and (3) the MnO-rich magnetites in unusual clasts are similar in chemical composition to those in carbonate clasts. Here I present a model for the formation of unusual clasts on the assumption that the clasts were produced from original carbonates by heating events. The model is summarized in Fig. 12, and the formational conditions are shown in Fig. 13. Original materials consisted of Ca-Mg-Fe carbonates with variable amounts of MnO-rich magnetite, apatite, and/or pyrrhotite (Fig. 12, and A in Fig. 13a). A unique clast (No. 41) of CaO-rich unusual type included MnO-rich-chlorites in addition to the above-stated minerals. As the MgO/(MgO+FeO) molecular ratios of periclase or PCA aggregate are 0.55–0.85, the original carbonates had the similar ratios. When the original materials for CaO-rich unusual clasts were heated, the carbonates decomposed into mono-oxides with loss of CO_2 component; siderite and magnesite components of the original carbonates decomposed to produce grains or fine-grained aggregates of FeO-bearing periclase (B in Fig. 13a),

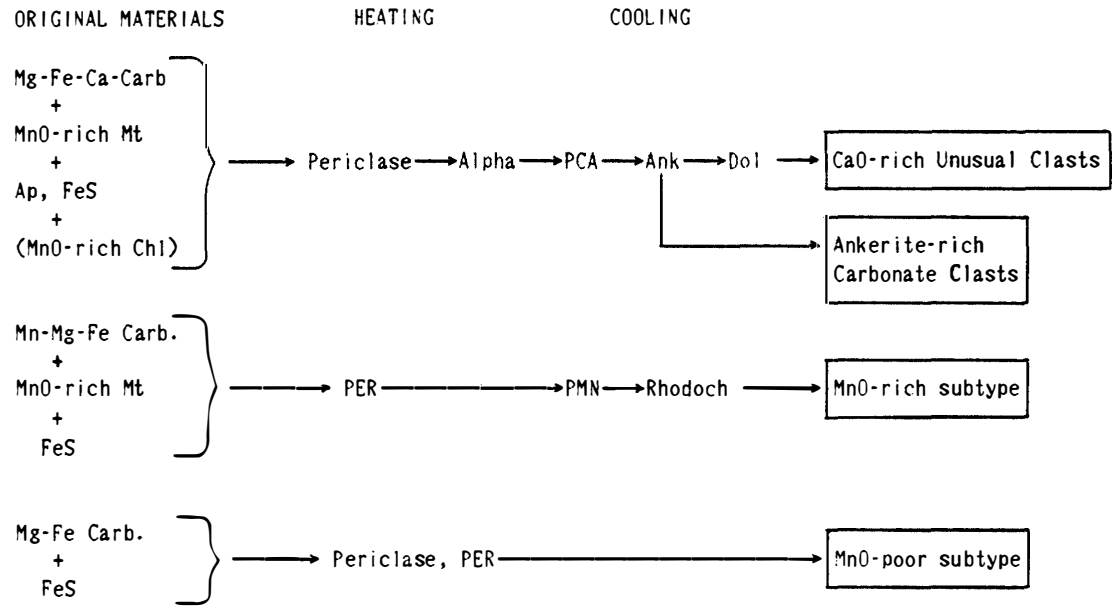

Fig. 12. Formation of CaO-rich unsual clasts, CaO-poor unusual clasts (MnO-rich and MnO-poor subtypes), and ankerite-rich carbonate clasts in Y-82162. Carb, Mt, Chl, Alpha, PCA, Ank, Dol, PER, PMN, and Rhodoch are carbonate, magnetite, chlorite, unknown Fe-Ca-S-O phase, fine-grained PCA aggregate, ankerite, dolomite, fine-grained PER aggregate, fine-grained PMN aggregate, and rhodochrosite, respectively.

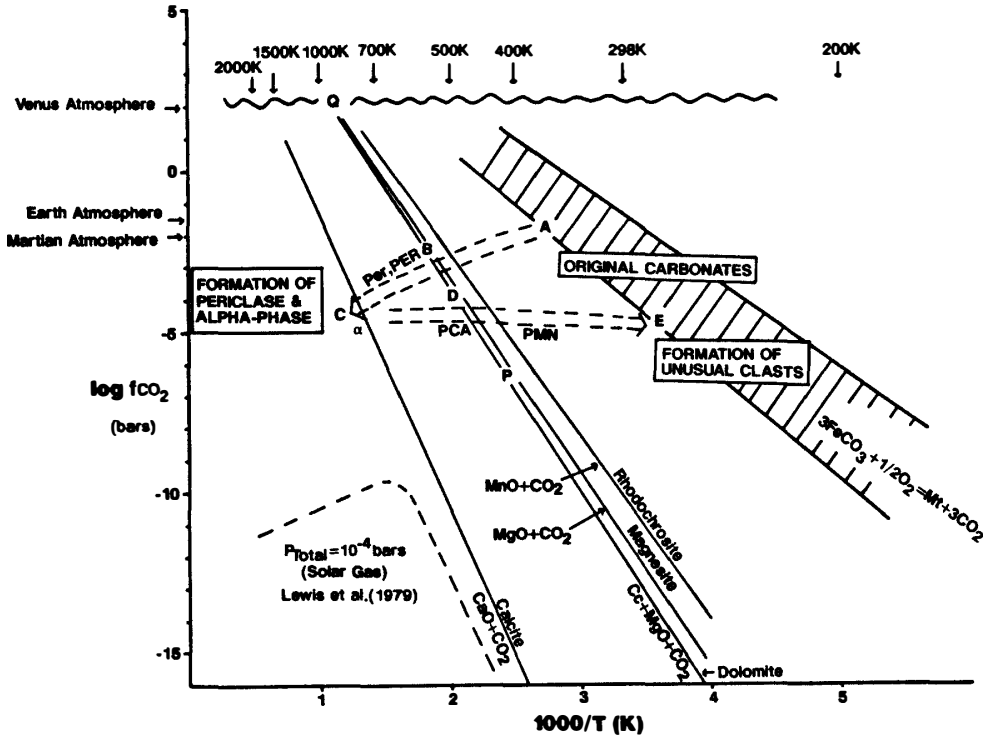

Fig. 13a. Formational conditions of unusual clasts. The thermodynamic data are quoted from ROBIE *et al. (1979). The hatched area is calculated using equation* $3FeCO_3+0.5O_2=Fe_3O_4+3CO_2$, *with a range of oxygen fugacity in which magnetite is stable (Fig. 13b), on the assumption that the* $FeCO_3$ *activity of carbonates is 0.15 (Fig. 7). The upper limit of* CO_2 *fugacity is assumed to be 150 bars which correspond to a pressure at the center of a body with 100 km radius. The* CO_2 *partial pressures of the solar gas with a total gas pressure of* 10^{-4} *bars (*LEWIS *et al., 1979) are shown by a dash-line for reference. A-B-C-D-E is a formational trend of unusual clasts; at point B periclase (Per) and PER aggregate begin to form, at point C alpha phase forms by decompositions of* $CaCO_3$, *and along C-D-E carbonitization takes place, resulting in the formation of PCA and PMN aggregates (see text). The lower limit P for the conditions of B and D corresponds to 420 K which is obtained in Fig. 13b, and the upper limit is point Q with 150 bars and about 900 K.*

and in the case that magnetites were included in the original materials, periclase overgrew on the magnetite grains (Photo 16). Further heating resulted in decomposition of calcite component of the original carbonates (C in Fig. 13a), and CaO produced reacted with the original FeS to form the alpha phase, which are rims overgrown on the FeO-bearing periclase. After the formation of periclase and alpha phase, cooling took place, resulting in carbonatization; the fine-grained aggregates of FeO-bearing periclase and probably the CaO component remained reacted with CO_2 component to produce Ca-rich carbonates, resulting in PCA aggregate (D in Fig. 13a). Then, ankerite precipitated to form the ankerite mantle, which was in turn rimmed by dolomites (E in Fig. 13a).

The original materials for MnO-rich type of CaO-poor unusual clasts consisted mainly of Mn-rich carbonates and FeS (Fig. 12). Heating of the original Mn-Mg-Fe carbonates produced heterogeneous mixtures of fine-graind PER aggregates and

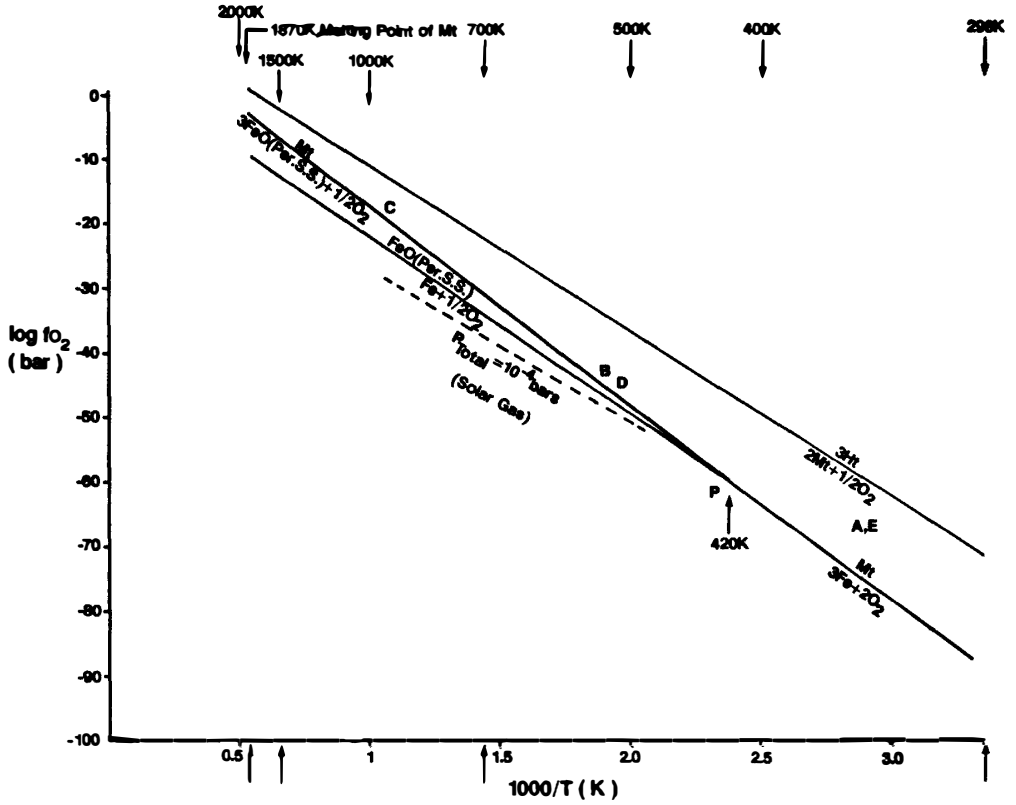

Fig. 13b. Formational conditions for FeO-bearing periclases coexisting with magnetites in unusual clasts. Thermodynamic data are quoted from ROBIE *et al. (1979). The solid line with B, C and D is reaction* $3FeO+0.5O_2=Fe_3O_4$ *(Mt), on the assumption that the FeO activity of periclase solid solution (Per. S. S.) is 0.30, and point P (420 K) is the lower limit for the reaction. The* O_2 *partial pressures of the solar gas with a total gas pressure of* 10^{-4} *bars are shown by a dash-line for reference. Points B and D (see Fig. 13a) must be within the temperature range from 420 K (P) to 900 K (Q in Fig. 13a), and the point C must be higher than B and D and lower that the melting temperature of magnetite (1870 K).*

fine-grained MnO-rich oxides (Fig. 13). Cooling of the oxide mixtures resulted in carbonatization, and rhodochrosite was produced from the fine-grained MnO-rich oxides, resulting in PMN aggregate.

The original materials for MnO-poor type of CaO-poor unusual clasts seem to be magnesites with a small amount of FeS (Fig. 12). The heating of the original Mg-Fe carbonates produced fine-grained aggregates of FeO-bearing periclase (PER aggregate).

The fugacity of CO_2 of original materials and during the formation of unusual clasts is not clear, but it is assumed in Fig. 13a that the fugacity was lower than the pressure at the center of a parent body with 100 km radius (about 150 bars). Periclase overgrowth on magnetites gives a constraint for the formational condition of unusual clasts (B in Fig. 13) as follows. On the assumption that the periclase with MgO/(MgO+FeO) mole ratio of 0.7 was in equilibrium with the magnetites during the formation of the periclase, the temperature and oxygen fugacity must be higher than 420 K and 10^{-60} bars, respectively (P in Fig. 13b). On the other hand, the upper limit of temperature is shown by Q in Fig. 13a, giving about 900 K. Therefore,

the points B and probably D must be within a temperature range from 420 to 900 K, as shown in Fig. 13a. The temperature of C in Fig. 13 should be lower than the melting point of magnetites (1870 K). The CO_2 fugacity of B and D in Fig. 13a must be in a range of 10^{-6} bars to 150 bars, which are much higher than that of a solar gas with a total pressure of 10^{-4} bars. Figure 13b shows that oxygen fugacity of B and D is also higher than that of a solar gas with a toal gas pressure of 10^{-4} bars.

These high values of CO_2 and O_2 fugacities suggest that the formation of unusual clasts took place in a parent body or in an extremely-oxidized gas. Most CaO-rich unusual clasts have thin dolomite rims of a constant width, suggesting that the dolomites precipitated on free surfaces of unusual clasts suspended in a fluidal phase (liquid or gas). The dolomites might be formed in a water reservoir of the parent body or in an oxidized gas localized in the solar nebula.

Terrestrial periclases occur in marbles which have suffered contact-metamorphism, and they are considered to have formed by decomposition of dolomites during the contact-metamorphism, but most of the periclases have changed to brucites by later hydration (WATANABE, 1935), suggesting that periclases are apt to react with H_2O to produce brucite. This suggestion is favorable for the latter possibility stated above that unusual clasts have formed in an oxidized gas, because periclases in unusual clasts have never reacted with H_2O to produce brucites. The temperature and H_2O fugacity of unusual clasts were within the condition of the left hand side of the reaction line for brucite in Fig. 14, and the unusual clasts have never been in a condition where liquid water was stable.

Recently ZINNER *et al.* (1990) found small periclase grains in a calcium-aluminum inclusion (CAI) from the Vigarano CV3 chondrite, and concluded that the periclase grains have an extraneous origin from a reservoir depleted in silicon. I agree with their conclusion and present a hypothesis that the periclase grains in the CAI were produced from carbonate precursors by heating events.

7.3. Formation of sodian talc-rich phyllosilicates

Sodian talc-rich phyllosilicates in sodian talc-rich clasts are extermely depleted in CaO and MnO contents; the molecular ratios of $CaO/AlO_{1.5}$ and MnO/FeO are lower than those of non-Antarctic CI chondrites (Table 3, Fig. 2a), suggesting that they were produced from the original materials which had already separeted carbonate and probably Mn-rich magnetite components (Fig. 11). The sodian talc component can be produced by the following equation;

$$\underset{\text{En}}{6MgSiO_3} + 0.5\underset{\text{Ab}}{NaSi_3AlO_8} + 2H_2O \longrightarrow \underset{\text{Sodian talc}}{Na_{0.5}Mg_6Si_{7.5}Al_{0.5}O_{20}(OH)_4}, \qquad (2)$$

where En and Ab are enstatite and albite, respectively. This reaction may take place under conditions similar to the reaction line for talc shown in Fig. 14. Phyllosilicates in sodian talc-rich clasts have the average Mg/(Mg+Fe) atomic ratio of 0.86, and small amounts of MgO in eq. (2) should be substituted by FeO although some parts of Fe may be ferric.

Veins in matrix-like and composite clasts consist of sodian talc-rich phyllosilicates (Fig. 4a), but they are rather intermediate between sodian talc-rich phyllosilicates and

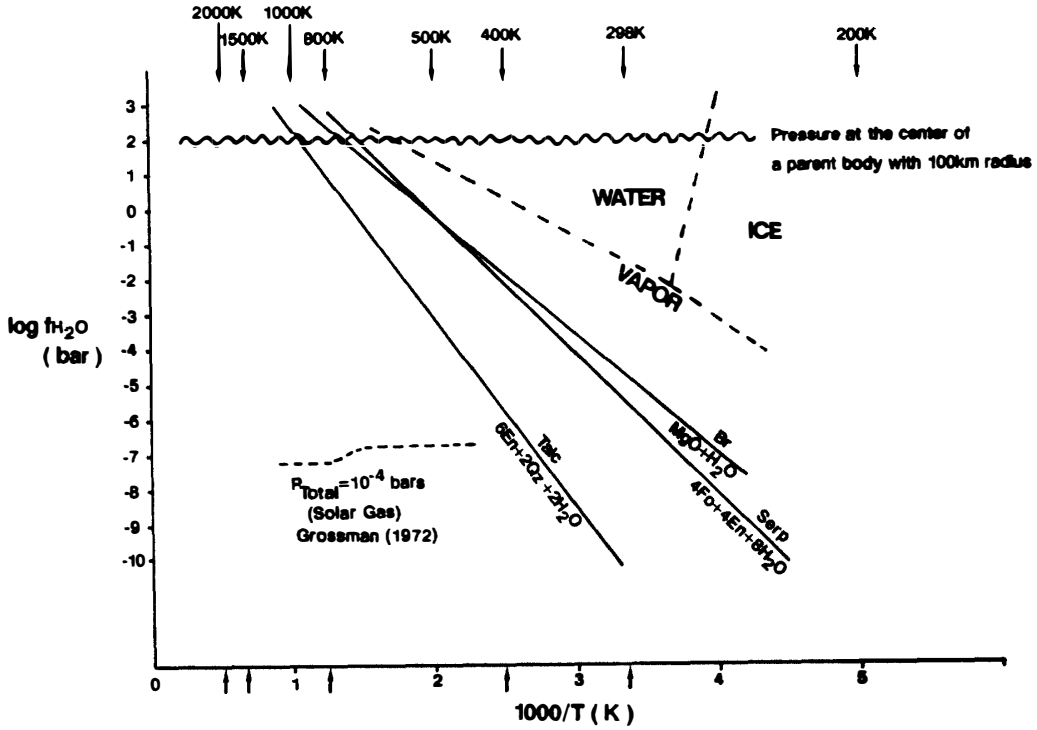

Fig. 14. Formational conditions of talc (Talc), chrysotile (Serp), and brucite (Br) with a phase diagram for pure H_2O. The thermodynamic data are quoted from ROBIE *et al. (1979). The H_2O partial pressures of the solar gas with a total gas pressure of 10^{-4} bars (*GROSSMAN, *1972) are shown by a dash-line for reference. Fo, En and Qz are forsterite, enstatite and silica, respectively.*

chlorite-rich phyllosilicates (Fig. 4b). Their occurrence (Photos 8 and 26) shows that they were produced from a fluidal phase (liquid or gas) which had transported the enstatite and albite components of eq. (2).

7.4. Formation of chlorite-rich phyllosilicates

FeO-rich chlorites in reaction zones between phyllosilicates and magnetites in composite and matrix-like clasts have been formed by eq. (1), and FeO-rich chlorites in magnetite clasts were also produced by eq. (1) from the original phyllosilicates similar to those in chlorite-rich clasts. The phyllosilicates in chlorite-rich and matrix-like clasts have unique textures, amygdule, network, and microspherules (Photos 4, 5, 6, and 7). The amygdule texture is observed as a gas cavity or vesicle in terrestrial volcanic rocks, which is filled by secondary minerals such as calcite, quartz, chalcedony, and/or zeolites, but the center of amygdule textures in chlorite-rich clasts is vacant (Photo 4). The phyllosilicates in chlorite-rich clasts were probably produced through a fluidal phase (liquid or gas). In addition to this, chlorite-rich clasts include magnesian chlorites (or serpentine) with Mg/(Mg+Fe) atomic ratios up to 0.86 (Fig. 3a), and this magnesian chlorites (or serpentine) cannot be produced only by eq. (1). The microspherules of chlorites in matrix-like clasts show a centroradial core with a thin rind (Photo 7), and this texture might be produced by replacement of

olivine or pyroxene (WATANABE *et al.*, 1988). These suggest a reaction to produce a chlorite (or serpentine) component of the chlorite-rich phyllosilicates;

$$\underset{\text{Olivine}}{4(Mg, Fe)_2SiO_4} + \underset{\text{Pyroxene}}{4(Mg, Fe)SiO_3} + 8H_2O \longrightarrow \underset{\text{Chlorite (or Serpentine)}}{(Mg, Fe)_{12}Si_8O_{20}(OH)_{16}} . \quad (3)$$

The relationship between temperature and H_2O fugacity for eq. (3) is not known, but it may be similar to that for chrysotile shown in Fig. 14. The reaction temperature for eq. (3) seems to be lower than that for eq. (2), which is in accord with the fact that the grain sizes of the phyllosilicates in sodian talc-rich clasts are larger than those of the phyllosilicates in chlorite-rich clasts and matrix-like clasts. Namely, sodian talc-rich phyllosilicates were produced in hotter regions of the parent body, and chlorite-rich phyllosilicates in chlorite-rich clasts and matrix-like clasts were formed in cooler regions near the surface of the parent body. The network in matrix-like clasts may have formed *in situ* through a fluidal phase (liquid or gas) bearing the olivine and pyroxene components of eq. (3).

7.5. Heating events

AKAI (1989) and TOMEOKA *et al.* (1989) reported that some phyllosilicates in Y-82162 include submicroscopic olivine grains and concluded that the olivines were produced from the host phyllosilicates by a heating event. The discussion that reaction (1) had produced FeO-rich chlorites in composite clasts suggests that weak heating might have taken place after the formation of composite clasts. Considering that the unusual clasts were produced by heating events, most kinds of clasts in Y-82162 may have more or less suffered heating in the nebula and/or the parent body. On the other hand, the anhydrous chondritic fragments seem not to have suffered any heating, and the heating events have ceased prior to the regolith gardening on the Y-82162 parent body.

Taking into account that periclase grains occur in a Ca- and Al-rich inclusion from the Vigarano CV chondrite (ZINNER *et al.*, 1990), the heating events which were relevant to the formation of unusual clasts and submicroscopic olivine grains in phyllosilicate clasts in Y-82162 might be due to the shock impacts by collision of planetesimals induced by supernovae (CLAYTON *et al*, 1973; LATTIMER *et al.*, 1978).

8. Conclusions

(1) Unusual clasts include FeO-bearing periclases. They were produced by heating events from carbonate-rich precursors probably in an oxidized gas of high CO_2 and O_2 fugacities.

(2) Most of carbonate clasts were produced at the stage corresponding to the carbonate mantles of unusual clasts, although some of them could be the carbonate-rich precursors of the unusual clasts.

(3) Sodian talc-rich clasts were probably produced from enstatite- and albite-rich precursors in the hot and deep interiors of the parent body.

(4) Phyllosilicates in chlorite-rich clasts, magnetite clasts and matrix-like clasts show unique microtextures; amygdule, network-like, and microspherulitic, and the

three clast-types were probably produced from olivine- and pyroxene-rich precursors in shallow levels of the parent body.

(5) Composite clasts consist of two or more clast-types, and they were produced on the parent body by impacts.

(6) Matrix-like and composite clasts are sometimes cut across by sodian talc-rich phyllosilicate veins, compositions of which are intermediate between those of sodian talc-rich and chlorite-rich clasts. The veins may have formed in cracks by a fluidal phase, which had come from the interior where the sodian talc-rich clasts were produced.

(7) The matrix of Y-82162 consists mainly of FeO-rich chlorites (or serpentines) which occur as fine-grained massive aggregates. The matrix chlorites (or serpentines) may have been produced by eq. (1).

(8) Anhydrous chondritic fragments were projectiles which collided on the parent body to produce the regolith breccia of Y-82162. Some seem to be ordinary chondritic materials, and they have never experienced any hydration on the Y-82162 parent body.

Acknowledgments

The consortium on the Antarctic carbonaceous chondrites with CI affinities, Y-82162, Y-86720, and B-7904 has been approved by National Institute of Polar Research (NIPR) in September 1987, and I thank NIPR and Drs. K. YANAI and H. KOJIMA of NIPR for the sample allotment and help to the consortium. I also thank Dr. K. TOMEOKA of Tokyo University for the discussion on Y-82162 and anonymous referees for their kind suggestions and revision of the manuscript. This study has been supported by a Grant-in-Aid for Scientific Research, from the Ministry of Education, Science and Culture.

References

AKAI, J. (1989): Mineralogical evidence of heating events in carbonaceous chondrites. Papers Presented to the 14th Symposium on Antarctic Meteorites, June 6–8, 1989. Tokyo, Natl Inst. Polar Res., 22–23.

AKAI, J. (1990): Thermal metamorphism in four Antarctic carbonaceous chondrites and its temperature scale estimated by T-T-T diagram. Papers Presented to the 15th Symposium on Antarctic Meteorites, May 30–June 1, 1990. Tokyo, Natl Inst. Polar Res., 86–87.

BISCHOFF, A. and METZLER, K. (1990): Petrography and chemistry of the three carbonaceous chondrites Y-86720, Y-82162, and B-7904. Papers Presented to the 15th Symposium on Antarctic Meteorites, May 30–June 1, 1990. Tokyo, Natl Inst. Polar Res., 185–187.

CLAYTON, R. N. and MAYEDA, T. K. (1989): Oxygen isotopic classification of carbonaceous chondrites. Lunar and Planetary Science, XX. Houston, Lunar Planet. Inst., 169–170.

CLAYTON, R. N., GROSSMAN, L. and MAYEDA, T. K. (1973): A component of primitive nuclear composition in carbonaceous meteorites. Science, **182**, 485–488.

EBIHARA, M. and SHINONAGA, T. (1989): Chemical compositions of some primitive carbonaceous chondrites from Antarctica. Papers Presented to the 14th Symposium on Antarctic Meteorites, June 6–8, 1989. Tokyo, Natl Inst. Polar Res., 35–36.

GROSSMAN, L. (1972): Condensation in the primitive solar nebula. Geochim. Cosmochim. Acta, **36**, 597–619.

IKEDA, Y. (1989): Petrochemical study of the Yamato-691 enstatite chondrite (E3) III: Description and mineral compositions of chondrules. Proc. NIP R Symp. Antarct. Meteorites, **2**, 75–108.

IKEDA, Y. (1990): Mineralogy of clasts in the Y-82162 chondrite (CI). Papers Presented to the 15th Symposium on Antarctic Meteorites, May 30–June 1, 1990. Tokyo, Natl Inst. Polar Res., 81–82.

KALLEMEYN, G. W. (1988): Compositional study of carbonaceous chondrites with CI-CM affinities. Papers Presented to the 13th Symposium on Antarctic Meteorites, June 7–9, 1988. Tokyo, Natl Inst. Polar Res., 132–134.

KOJIMA, H. and YANAI, K. (1987): Yamato-82162; Possible first Cl carbonaceous chondrite from Antarctica. Papers Presented to the 12th Symposium on Antarctic Meteorites, June 8–10, 1987. Tokyo, Natl Inst. Polar Res., 15.

LATTIMER, J. M., SCHRAMM, D. N. and GROSSMAN, L. (1978): Condensation in Supernova ejecta and isotopic anomalies in meteorites. Astrophys. J., **219**, 230–249.

LEWIS, J. S., BARSHAY, S. S. and NOYES, B. (1979): Primordial retension of carbon by the terrestrial planets. Icarus, **37**, 190–206.

MAYEDA, T. and CLAYTON, R. N. (1987): Oxgen isotopic compositions of several Antarctic meteorites. Mem. Natl Inst. Polar Res., Spec. Issue, **46**, 144–150.

MAYEDA, T. K. and CLAYTON, R. N. (1990): Oxygen isotopic compositions of B-7904, Y-82162, and Y-86720. Papers Presented to the 15th Symposium on Antarctic Meteorites, May 30–June 1, 1990. Tokyo, Natl Inst. Polar Res., 196–197.

MIYAMOTO, M. (1990): Midinfrared diffuse reflectance spectra of some Antarctic carbonaceous chondrites. Papers Presented to the 15th Symposium on Antarctic Meteorites, May 30–June 1, 1990. Tokyo, Natl Inst. Polar Res., 89–91.

PAUL, R. L. and LIPSCHUTZ, M. E. (1989): Consortium report on carbonaceous chondrites from Queen Maud Land, Antarctica: Glimpses of new parents. Papers Presented to the 14th Symposium on Antarctic Meteorites, June 6–8, 1990. Tokyo, Natl Inst. Polar Res., 32–33.

PAUL, R. L. and LIPSCHUTZ, M. E. (1990): Consortium study of labile trace elements in some Antarctic carbonaceous chondrites: Antarctic and non-Antarctic meteorite comparisons. Proc. NIP R Symp. Antarct. Meteorites, **3**, 80–95.

ROBIE, R. A., HEMINGWAY, B. S. and FISHER, J. R. (1979): Thermodynamic properties of minerals and related substances at 298. 15 K and 1 bar (10^5 Pascals) pressure and at higher temperatures. Geol. Surv. Bull., **1452**, 456 p.

SCHREYER, W., ABRAHAM, K. and KULKE, H. (1980): Natural sodium phlogopite coexisting with potassium phlogopite and sodian aluminum talc in a metamorphic evaporite sequence from Derrag, Tell Atlas, Algeria. Contrib. Mineral. Petrol., **74**, 223–233.

TOMEOKA, K. (1990a): The origin of phyllosilicates in the Yamato-82162 CI carbonaceous chondrite. Papers Presented to the 15th Symposium on Antarctic Meteorites, May 30–June 1, 1990. Tokyo, Natl Inst. Polar Res., 83–85.

TOMEOKA, K. (1990b): Phyllosilicates veins in a CI meteorite: Evidence for aqueous alteration on the parent body. Nature, **345**, 138–140.

TOMEOKA, K. and BUSECK, P. (1988): Matrix mineralogy of the Orgueil CI carbonaceous chondrite. Geochim. Cosmochim. Acta, **52**, 1627–1640.

TOMEOKA, K., KOJIMA, H. and YANAI, K. (1988): Yamato-82162: A new kind of CI carbonaceous chondrite found in Antarctica. Papers Presented to the 13th Symposium on Antarctic Meteorites, June 7–9, 1988. Tokyo, Natl Inst. Polar Res., 126–127.

TOMEOKA, K., KOJIMA, H. and YANAI, K. (1989): Yamato-82162: A new kind of CI carbonaceous chondrite found in Antarctica. Proc. NIPR Symp. Antarct. Meteorites, **2**, 36–54.

WATANABE, S., TSUCHIYAMA, A. and KITAMURA, M. (1988): A preliminary report of mineralogy of Y-82162 (CI). Papers Presented to the 13th Symposium on Antarctic Meteorites, June 7–9, 1988. Tokyo, Natl Inst. Polar Res., 128–129.

WATANABE, T. (1935): On the brucite-marble (predazzite) from the Nantei mine, Suian, Tyosen (Korea). J. Fac. Sci., Hokkaido Imperial Univ., Ser. 4, **III**(1), 49–67.

YAMAMOTO, Y. and NAKAMURA, N. (1989): Chemical characteristics and their inference to classifica-

tion of Yamato-82162 and -86720 meteorites. Papers Presented to the 14th Symposium on Antarctic Meteorites, June 6–8, 1989. Tokyo, Natl Inst. Polar Res., 27–29.

ZINNER, E. K., CAILLE, C. and EL GORESY, A. (1990): Evidence of extraneous origin of a periclase-metal fremdling from the Vigarano CV3 chondrite. Earth Planet. Sci. Lett. (in press).

(*Received August 1, 1990; Revised manuscript received November 1, 1990*)